Report

Current Biology

Region-specific nucleus accumbens dopamine signals encode distinct aspects of avoidance learning

Graphical abstract

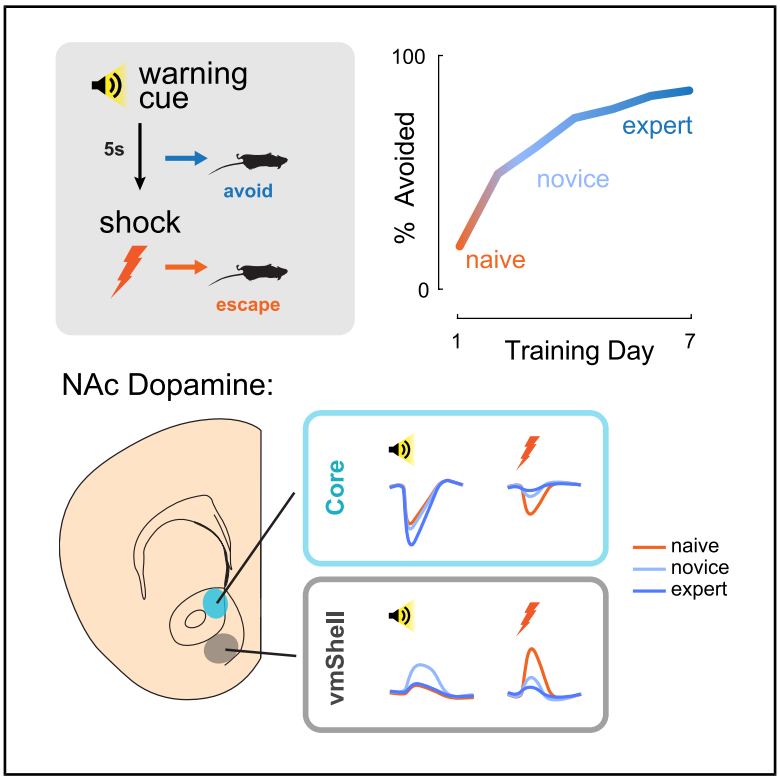

Authors

Gabriela C. Lopez, Louis D. Van Camp, Ryan F. Kovaleski, Michael D. Schaid, Venus N. Sherathiya, Julia M. Cox, Talia N. Lerner

Correspondence

talia.lerner@northwestern.edu

In brief

Lopez et al. show that NAc Core and vmShell dopamine signals display distinct dynamics during active avoidance learning and in response to inescapable shocks. These data provide avenues to understand how heterogeneous dopamine subpopulations work together to represent aversive stimuli and allow animals to learn to avoid danger in their environment.

Highlights

- Core and vmShell dopamine display distinct dynamics during avoidance learning
- Core dopamine responses to warning cues strengthen during expert performance
- vmShell dopamine responses to shocks and cues are present early but later fade
- Escapable and inescapable shock protocols elicit distinct dopamine responses

Lopez et al., 2025, Current Biology *35*, 1–11
May 19, 2025
https://doi.org/10.1016/j.cub.2025.04.006

CellPress

Current Biology

CellPress
OPEN ACCESS

Report

Region-specific nucleus accumbens dopamine signals encode distinct aspects of avoidance learning

Gabriela C. Lopez,[1,2] Louis D. Van Camp,[1] Ryan F. Kovaleski,[1] Michael D. Schaid,[1] Venus N. Sherathiya,[1] Julia M. Cox,[1] and Talia N. Lerner[1,2,3,*]

[1]Department of Neuroscience, Northwestern University Feinberg School of Medicine, Chicago, IL 60611, USA
[2]Northwestern University Interdepartmental Neuroscience Program (NUIN), Evanston, IL 60208, USA
[3]Lead contact
*Correspondence: talia.lerner@northwestern.edu
https://doi.org/10.1016/j.cub.2025.04.006

SUMMARY

Avoidance learning—learning to avoid bad outcomes—is an essential survival behavior. Dopamine signals are widely observed in response to aversive stimuli, indicating they could play a role in learning about how to avoid these stimuli.[1–5] However, it is unclear what computations dopamine signals perform to support avoidance learning. Furthermore, substantial heterogeneity in dopamine responses to aversive stimuli has been observed across nucleus accumbens (NAc) subregions.[3,6–8] To understand how heterogeneous dopamine responses to aversive stimuli contribute to avoidance learning, we recorded NAc core (Core) and NAc ventromedial shell (vmShell) dopamine during a task in which mice could avoid a footshock punishment by moving to the opposite side of a 2-chamber apparatus during a 5-s warning cue. Both signals evolved substantially—but differently—with learning. We found that Core and vmShell dopamine signals responded oppositely to shocks at the beginning of training and oppositely to warning cues as cue-shock associations developed in mid-training. Core dopamine responses strengthen with learning and are especially evident during expert performance. vmShell dopamine responses to cues and shocks were present during early learning but were not sustained during expert performance. Our data support a model in which Core dopamine encodes prediction errors that guide the consolidation of avoidance learning, while vmShell dopamine guides initial cue-shock associations by signaling aversive salience.

RESULTS

Rapid acquisition of an active avoidance task with stable reaction times

Avoidance learning is a form of instrumental learning in which animals learn from negative reinforcement (removal of something bad). It is essential for survival but can become maladaptive when performed in excess, as in anxiety disorders, obsessive-compulsive disorder (OCD), and depression.[9,10] Dopamine is well known to be essential for instrumental learning, but it is best studied in the context of positive reinforcement (receipt of something good).[11,12] However, dopamine neurons respond not only to rewarding but also to aversive stimuli and associated cues,[1–5] raising the possibility that they play an important role in learning aversive associations to facilitate the performance of avoidance actions. Available evidence supports a role for dopamine in avoidance learning,[13–17] but the region specificity and evolution of dopamine responses during learning remain in question.[18]

To determine how nucleus accumbens (NAc) dopamine signals contribute to avoidance learning, we expressed the fluorescent dopamine sensor dLight1.3b in NAc core (Core) or ventromedial shell (vmShell)—two subregions known to respond differently when animals are exposed to inescapable aversive stimuli[3,6–8]—and implanted an optical fiber for *in vivo* fiber photometry recordings (Figures 1A, 1B, S1A, and S1B). After recovery from surgery, we trained mice to avoid a footshock punishment (0.4 mA) by moving to the opposite side of a 2-chamber apparatus during a 5-s warning cue. Movement to the opposite side of the chamber within 5 s of cue start resulted in cue cessation and shock avoidance. Failure to move to the opposite side of the chamber within 5 s resulted in shock delivery that continued until the mouse moved to the opposite side of the chamber (Figure 1C). Mice completed 30 trials daily for 7 days. Mice rapidly learned to avoid shocks, reaching an average of 85% avoidance by day 7 ($n = 36$, 85.10% ± 7.79%; Figure 1D). The latency to cross to the opposite chamber decreased over days ($F_{3.764,\ 131.7} = 91.49$, $p < 0.0001$; Figure 1E). However, the latencies to cross by trial type were remarkably stable after day 1 (Figure S2A). Mice displayed a bimodal shift from 5–6 s to 2–3 s across latencies over days (Figure S2B), suggesting that they shift discretely and follow a stable avoidance strategy. Sex differences in avoidance behavior were not apparent (Figures S3A–S3C).

Since cue-shock pairings can induce freezing as a fear response, we quantified freezing. We found that mice freeze during the task but decrease their freezing across days ($n = 25$, $F_{6,\ 294} = 17.22$, $p < 0.0001$). Freezing decreased strongly across days for the intertrial interval (ITI) period ($r = -0.97$, $p = 0.0003$), indicating that mice learned the ITI period was safe (Figure 1F).

Please cite this article in press as: Lopez et al., Region-specific nucleus accumbens dopamine signals encode distinct aspects of avoidance learning, Current Biology (2025), https://doi.org/10.1016/j.cub.2025.04.006

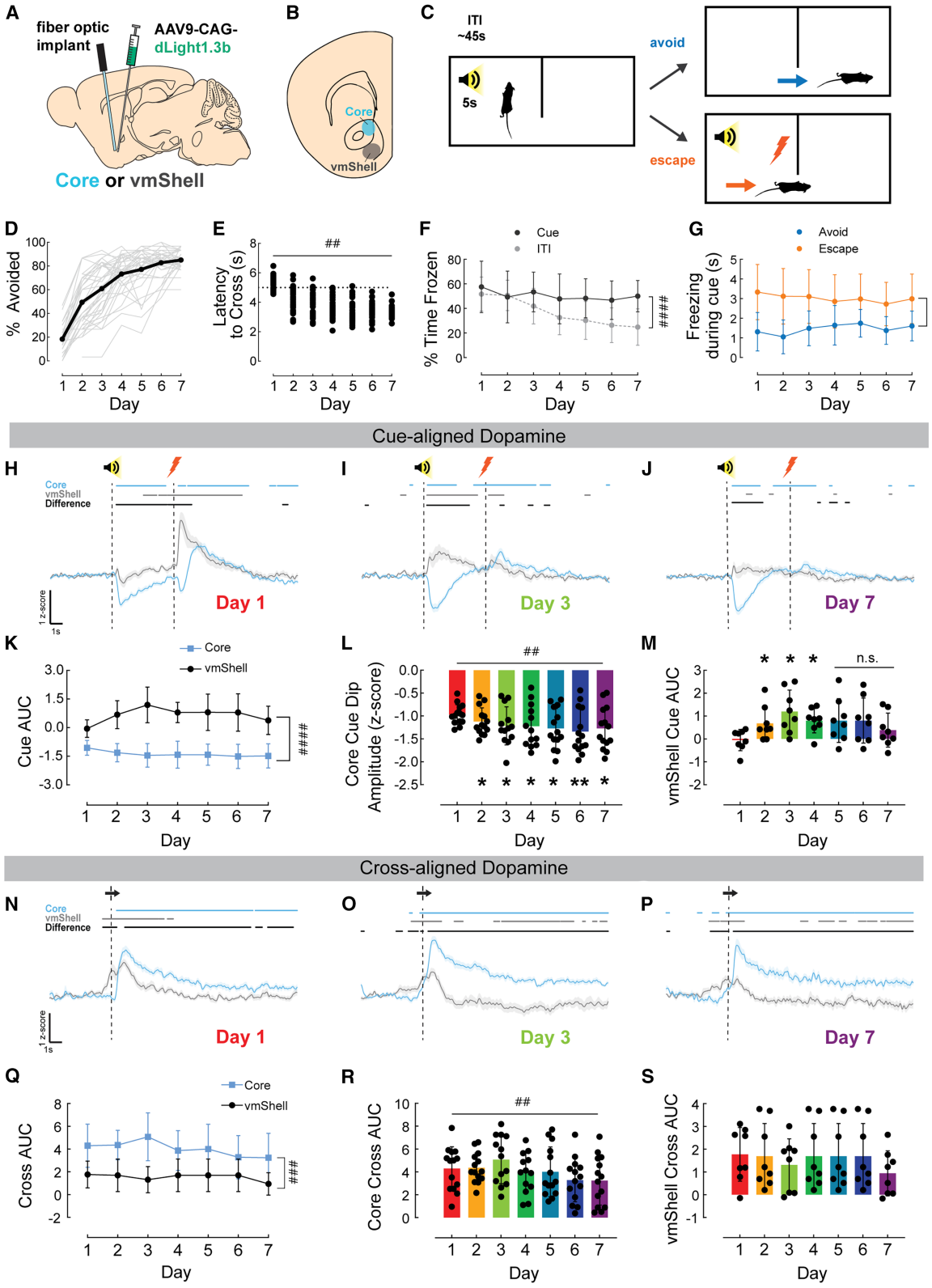

Figure 1. Rapid acquisition of active avoidance learning with distinct Core and vmShell dopamine responses

(A) Mice were injected with an adeno-associated virus (AAV) to express dLight1.3b in the Core or vmShell, and a fiber optic was placed at the same site to allow collection of fluorescent signals by fiber photometry.

(legend continued on next page)

Please cite this article in press as: Lopez et al., Region-specific nucleus accumbens dopamine signals encode distinct aspects of avoidance learning, Current Biology (2025), https://doi.org/10.1016/j.cub.2025.04.006

Although freezing trended lower across days for the cue period ($r = -0.67$, $p = 0.099$), it remained significantly higher than for the ITI period, indicating that mice still displayed fear responses to the cue throughout training. Mice froze more on escape than on avoid trials ($F_{1,\ 1,115} = 265.6$, $p < 0.0001$; Figure 1G), indicating that a major reason mice fail to avoid shocks is because of their competing intuition to freeze. Taken together, these data show that the mice learn the cue-shock association robustly and then mostly overcome initial freezing responses to learn adaptive active avoidance behaviors by negative reinforcement.

Core and vmShell have distinct dopamine responses during active avoidance learning

To assess region-specific dopamine signals during active avoidance learning, dopamine release dynamics in the Core and vmShell were recorded across all 7 days of the task and processed using standard pipelines for fiber photometry data (Figure S1C).[4,19] Bootstrapped confidence interval (CI) waveform analyses (95% CI) were conducted to identify significant deviations from baseline in fiber photometry signals (defined as when the bounds of the 95% CIs did not include 0) and to determine when Core and vmShell signals differed (defined as when the bounds of the 95% CI did not overlap). Core and vmShell dopamine signals aligned to the warning cue were distinct and evolved across days (Figures 1H–1J). We also quantified the area under the curve (AUC) for Core and vmShell dopamine signals during the cue but prior to avoidance crossing (0–2 s post-cue; average avoidance cross time 2.89 ± 0.49 s) and found a significant main effect of brain region (Core $n = 14$, vmShell $n = 8$, $F_{1,\ 20} = 64.78$, $p < 0.0001$) and day ($F_{3.892,\ 76.54} = 3.387$, $p = 0.0140$), with a significant interaction between the two factors ($F_{6,\ 118} = 10.95$, $p < 0.0001$; Figure 1K).

Core dopamine showed negative-going responses (“dips”) to the warning cue, which grew larger over days ($F_{3.150,\ 39.90} = 6.302$, $p = 0.0011$; Figure 1L). By contrast, vmShell dopamine signals showed an oppositely signed and more complex pattern of change. Cue AUC (0–2 s) for vmShell dopamine was minimal on day 1, grew over the first few days of training, and then decreased later in training (main effect of day, $F_{2.791,\ 19.54} = 5.677$, $p = 0.0065$, with differences from day 1 appearing on days 2, 3, and 4; Figure 1M). Sex differences in these dopamine signals were largely not observed, except for slightly larger and

(B) Schematic showing the targeted areas for Core (blue) and vmShell (gray).
(C) Schematic of the active avoidance task. A 5-s warning cue was played. If the mouse crossed into the opposite chamber before 5 s elapsed, the cue turned off, and the mouse avoided receiving a shock on that trial (avoid trials). If the mouse did not cross into the opposite chamber before 5 s elapsed, shock began. Shock ended when the mouse crossed into the opposite chamber (escape trials). Thirty trials were given per day across 7 days, with an average intertrial interval of 45 s.
(D) Performance on the active avoidance task was measured by the percent of shocks avoided across the 7 days of training ($n = 36$). By day 7, mice, on average, avoided ~85% of shocks. The black line shows the average for all mice in the study. The gray lines represent the performance of individuals.
(E) Latency to cross to safety over days of active avoidance training ($n = 36$). Each dot is the average for the day from an individual mouse. Latency to cross decreased over days of active avoidance (repeated measures one-way ANOVA; $F_{3.764,\ 131.7} = 91.49$, $p < 0.0001$). The dotted line at 5 s indicates the latency at which shock would begin. Hash symbol (#) indicates main effects. Error bars are SD.
(F) Percentage of time frozen during the cue (black line) and intertrial interval (ITI, gray dashed line) over days of active avoidance ($n = 25$). Each black square (cue) or gray circle (ITI) represents the average percent freezing of all mice for that day. Percentage of freezing between cue and ITI are significantly different: mixed-effects analysis; $F_{6,\ 294} = 17.22$, $p < 0.0001$ (day); $F_{1,\ 49} = 19.61$, $p < 0.001$ (Cue versus ITI); $F_{6,\ 147} = 9.845$, $p < 0.0001$ (day × Cue versus ITI). Freezing decreased across days for the ITI period (correlation; $r = -0.97$, $p = 0.0003$) and trended lower across days for cue period (correlation; $r = -0.67$, $p = 0.099$). Hash symbol (#) indicates main effects, and asterisk (*) indicates post hoc comparisons. Error bars are SD.
(G) Freezing duration for escape trials (orange) and avoid trials (blue) over days of active avoidance ($n = 25$). Each dot represents the average freezing duration for all mice for that day. Freezing duration during the cue in avoid versus escape trials is significantly different (mixed-effects analysis; $F_{1,\ 1,115} = 265.6$, $p < 0.0001$). Hash symbol (#) indicates main effects. Error bars are SD.
(H–J) Plots showing the dopamine signals collected from Core (blue) and vmShell (gray) aligned to the start of the warning cue (first dotted line). Shock occurred 5 s after the warning cue start on escape trials (second dotted line). Days 1 (H), 3 (I), and 7 (J) are shown. For (H)–(J), significant deviations from baseline in fiber photometry signals (defined as when the bounds of the 95% CIs did not include 0) are shown as blue or gray lines for Core or vmShell, respectively, above each plot. The black line indicates significant differences between Core and vmShell (defined as when the bounds of the 95% CI did not overlap).
(K) The area under the curve (AUC) for the cue period (0–2 s) is shown for Core (blue) and vmShell (gray) across days. Cue AUC for Core and vmShell are significantly different: mixed-effects analysis; $F_{1,\ 20} = 64.78$, $p < 0.0001$ (brain region); $F_{3.892,\ 76.54} = 3.387$, $p = 0.0140$) (day); $F_{6,\ 118} = 10.95$, $p < 0.0001$ (brain region × day). Hash symbol (#) indicates main effects. Error bars are SD.
(L) Peak negative-going amplitude (cue dip amplitude) for Core over days. Days 2–7 are significantly different from day 1: mixed-effects analysis; $F_{3.150,\ 39.90} = 6.302$, $p = 0.0011$ (day); Tukey’s comparisons, day 1 versus day 2, $p = 0.0377$, day 1 versus day 3, $p = 0.0239$, day 1 versus day 4, $p = 0.0432$, day 1 versus day 5, $p = 0.0201$, day 1 versus day 6, $p = 0.0070$, day 1 versus day 7, $p = 0.0404$. Hash symbol (#) indicates main effects, and asterisk (*) indicates post hoc comparisons. Error bars are SD.
(M) Cue AUC for vmShell over days. Days 2–4 are significantly different from day 1 (repeated measures one-way ANOVA; $F_{2.791,\ 19.54} = 5.677$, $p = 0.0065$; Tukey’s comparisons: days 1 versus 2, $^*p = 0.0480$, days 1 versus 3, $^*p = 0.0164$, days 1 versus 4, $^*p = 0.0192$. Hash symbol (#) indicates main effects, and asterisk (*) indicates post hoc comparisons. Error bars are SD.
(N–P) Plots showing the dopamine signals collected from Core (blue) and vmShell (gray) aligned to the time of crossing to the opposite chamber (dotted line). Days 1 (N), 3 (O), and 7 (P) are shown. For (N)–(P), significant deviations from baseline in fiber photometry signals (defined as when the bounds of the 95% CIs did not include 0) are shown as blue or gray lines for Core or vmShell, respectively, above each plot. The black line indicates significant differences between Core and vmShell (defined as when the bounds of the 95% CI did not overlap).
(Q) The AUC for the post-crossing period (0–5 s) is shown for Core (blue) and vmShell (gray) across days. Cross AUC for Core and vmShell are significantly different (mixed-effects analysis; $F_{4.423,\ 86.99} = 2.506$, $p = 0.0424$ [day]). Hash symbol (#) indicates main effects. Error bars are SD.
(R and S) Cross AUC for Core (R) and vmShell (S) are shown across days. Cross AUC for Core significantly changes across days (mixed-effects analysis; $F_{4.015,\ 50.86} = 4.147$, $p = 0.0055$). No significant changes are seen across days for vmShell (repeated measures one-way ANOVA; $F_{1.533,\ 10.73} = 0.9050$, $p = 0.407$). Hash symbol (#) indicates main effects, and asterisk (*) indicates post hoc comparisons. Error bars are SD.
Core $n = 14$, vmShell $n = 8$
See also Figures S1–S3.

Please cite this article in press as: Lopez et al., Region-specific nucleus accumbens dopamine signals encode distinct aspects of avoidance learning, Current Biology (2025), https://doi.org/10.1016/j.cub.2025.04.006

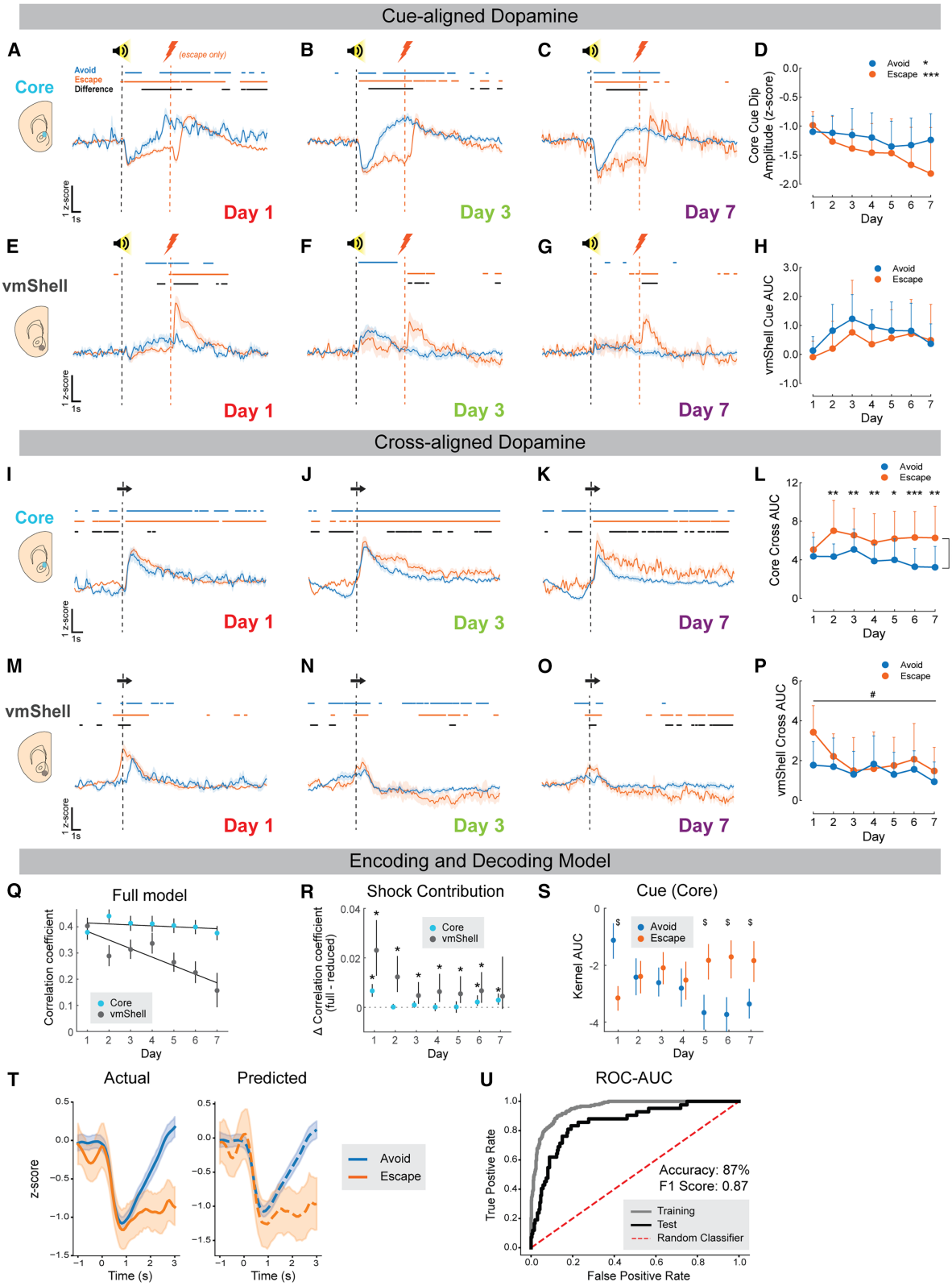

Figure 2. Core warning cue response dynamics differ by trial type while vmShell dopamine is excited by aversive outcomes

(A–C) Plots showing Core dopamine signals collected during avoid trials (blue) and escape trials (orange) from aligned to the start of the warning cue (first dotted line). Shock occurred 5 s after the warning cue start on escape trials (second dotted line). Days 1 (A), 3 (B), and 7 (C) are shown. For (A)–(C), significant deviations from

(legend continued on next page)

Please cite this article in press as: Lopez et al., Region-specific nucleus accumbens dopamine signals encode distinct aspects of avoidance learning, Current Biology (2025), https://doi.org/10.1016/j.cub.2025.04.006

more sustained vmShell cue signals in females (Figures S3D–S3J). These data indicate that Core and vmShell have distinct dopamine responses during active avoidance that evolve in unique ways across training.

To avoid or escape a shock, mice crossed to the opposite side of the chamber. Given the importance of this action, we assessed Core and vmShell dopamine release dynamics aligned to crossing. Dopamine signals for both the Core and vmShell increased at the time of crossing, but the responses were significantly different ($F_{4.423,\ 86.99} = 2.506$, $p = 0.0424$; Figures 1N–1Q). Core dopamine was better aligned to the crossing event, whereas vmShell dopamine began to increase earlier before crossing even early in training. Examining Core and vmShell separately, we found a main effect of day for Core ($F_{4.015,\ 50.86} = 4.147$, $p = 0.0055$; Figure 1R) but not for vmShell ($F_{1.533,\ 10.73} = 0.9050$, $p = 0.407$; Figure 1S), suggesting that Core dopamine specifically is involved in learning the value of the avoidance action over days.

Core warning cue response dynamics differ by trial type while vmShell dopamine is excited by aversive outcomes

While both avoid and escape events can be characterized as flight behaviors, they differ by a key feature—avoidance eliminates exposure to the shock while escape does not. Given this observation, we asked how dopamine signals in the Core and vmShell differ between avoid and escape trials in our task (Figure 2). After equivalent initial dips in Core dopamine in response to the cue, signals for avoid and escape trials diverged ~1.85 s post-cue (average time of significant divergence across days of training). Core dopamine dip amplitudes increased across days ($F_{6,\ 78} = 5.740$, $p < 0.0001$) for both avoid ($r = -0.81$, $p = 0.0282$; Figures 2A–2D) and escape trials ($r = -0.97$, $p = 0.0004$; Figures 2A–2D), indicating changing signals across learning. By contrast, vmShell dopamine aligned to the cue did not differ by trial type ($r = 0.06$, $p = 0.8995$ [avoid]; $r = 0.66$, $p = 0.1076$ [escape]; Figures 2E–2H). However, vmShell dopamine responded to shock onset in escape trials, indicating that vmShell dopamine is excited by aversive stimuli (Figures 2E–2G).

When aligned to crossing, Core dopamine dynamics during avoid versus escape trials slowly diverged over days (Figures 2I–2K). We found a significant main effect of trial type ($F_{1.000,\ 13.00} = 35.39$, $p < 0.0001$) with significant differences between avoid and escape trials emerging after day 1 (Figure 2L). Cross-aligned vmShell AUC showed significant effects across days, indicating evolving dynamics, but no significant effect of trial type ($F_{4.010,\ 28.07} = 3.234$, $p = 0.0265$ [day]; $F_{1.000,\ 7.000} = 2.112$, $p = 0.1894$ [trial type]; Figures 2M–2P).

baseline in fiber photometry signals (defined as when the bounds of the 95% CIs did not include 0) are shown as blue or orange lines for avoid or escape trials, respectively, above each plot. The black line indicates significant differences between avoid and escape (defined as when the bounds of the 95% CI did not overlap).
(D) Peak negative-going amplitude (cue dip amplitude) for the cue period (0–2 s) is shown for avoid and escape trials across days. Core dopamine dip amplitudes increased across days for both avoid (correlation; $r = -0.81$, $^{*}p = 0.0282$) and escape trials (correlation; $r = -0.97$, $^{***}p = 0.0004$). Error bars are SD.
(E–G) Plots showing vmShell dopamine signals collected during avoid trials (blue) and escape trials (orange) from aligned to the start of the warning cue. Days 1 (E), 3 (F), and 7 (G) are shown. For (E) and (F), significant deviations from baseline in fiber photometry signals (defined as when the bounds of the 95% CIs did not include 0) are shown as blue or orange lines for avoid or escape trials, respectively, above each plot. The black line indicates significant differences between avoid and escape (defined as when the bounds of the 95% CI did not overlap).
(H) The vmShell AUC for the cue period (0–2 s) is shown for avoid and escape trials across days. No significant differences are observed between avoid (correlation; $r = 0.06$, $p = 0.8995$) and escape trials (correlation; $r = 0.66$, $p = 0.1076$). Error bars are SD.
(I–K) Plots showing Core dopamine signals collected during avoid trials (blue) and escape trials (orange) aligned to the time of crossing to the opposite chamber (dotted line). Days 1 (I), 3 (J), and 7 (K) are shown. For I-K, significant deviations from baseline in fiber photometry signals (defined as when the bounds of the 95% CIs did not include 0) are shown as blue or orange lines for avoid or escape trials, respectively, above each plot. The black line indicates significant differences between avoid and escape (defined as when the bounds of the 95% CI did not overlap).
(L) The Core AUC for the post-crossing period (0–5 s) is shown for avoid and escape trials across days. Avoid and escape cross AUCs are significantly different from each other on days 2, 5, 6, and 7 (mixed-effects analysis; $F_{1.000,\ 13.00} = 35.39$, $p < 0.0001$; Tukey's comparisons, day 2 avoid versus escape, $p = 0.0043$, day 3 avoid versus escape, $p = 0.0069$, day 4 avoid versus escape, $p = 0.0023$, day 5 avoid versus escape, $p = 0.0182$, day 6 avoid versus escape, $p = 0.0009$, day 7 avoid versus escape, $p = 0.0013$). Hash symbol (#) indicates main effects, and asterisk (*) indicates post hoc comparisons. Error bars are SD.
(M–O) Plots showing vmShell dopamine signals collected during avoid trials (blue) and escape trials (orange) aligned to the time of crossing to the opposite chamber (dotted line). Days 1 (M), 3 (N), and 7 (O) are shown. For (M)–(O), significant deviations from baseline in fiber photometry signals (defined as when the bounds of the 95% CIs did not include 0) are shown as blue or orange lines for avoid or escape trials, respectively, above each plot. The black line indicates significant differences between avoid and escape (defined as when the bounds of the 95% CI did not overlap).
(P) The vmShell AUC for the post-crossing period (0–5 s) is shown for avoid and escape trials across days. A significant effect between days is observed but no significant effect of trial type: repeated measures two-way ANOVA; $F_{4.010,\ 28.07} = 3.234$, effect of day $p = 0.0265$ (day); $F_{1.000,\ 7.000} = 2.112$, $p = 0.1894$ (trial type). Hash symbol (#) indicates main effects. Error bars are SD.
(Q–S) Data points are the median of the bootstrapped distribution. Error bars are 95% CIs. (Q) Correlation coefficients over days for the full encoding models for Core and vmShell dopamine. The rate of change is estimated by fitting a line to each set of data points (Core slope = −0.004, $p = 0.437$; vmShell slope = −0.0327, $p = 0.008$). (R) The change in correlation coefficients when shock is removed as a behavioral event (full model − reduced model). Asterisks indicate that the difference in correlation coefficients is significantly different from 0 (dashed line; based on CIs with a Bonferroni correction for multiple comparisons). (S) Area under the curve (AUC) for the kernel values for avoid-cue and escape-cue over days. Dollar sign ($) indicates that the difference in AUC for the two events is >0 (based on CIs with a Bonferroni correction for multiple comparisons).
(T) Core dopamine signals during the cue period for avoid (blue) and escape (orange) trials on days 5–7. True signals are shown on the left (solid lines), and signals predicted to be avoid versus escape using the LSTM-FCN classification decoder are shown on the right (dashed lines).
(U) Receiver operator characteristic (ROC) curve for the LSTM-FCN classification decoder. The gray line represents the ROC of the training dataset, the black line represents the ROC of the test dataset, and the red dashed line represents random classification. Our decoding model achieved 87% accuracy with an AUC (ROC-AUC) of 0.86.
Core $n = 14$, vmShell $n = 8$
See also Figures S4–S6 and Tables S1–S3.

Please cite this article in press as: Lopez et al., Region-specific nucleus accumbens dopamine signals encode distinct aspects of avoidance learning, Current Biology (2025), https://doi.org/10.1016/j.cub.2025.04.006

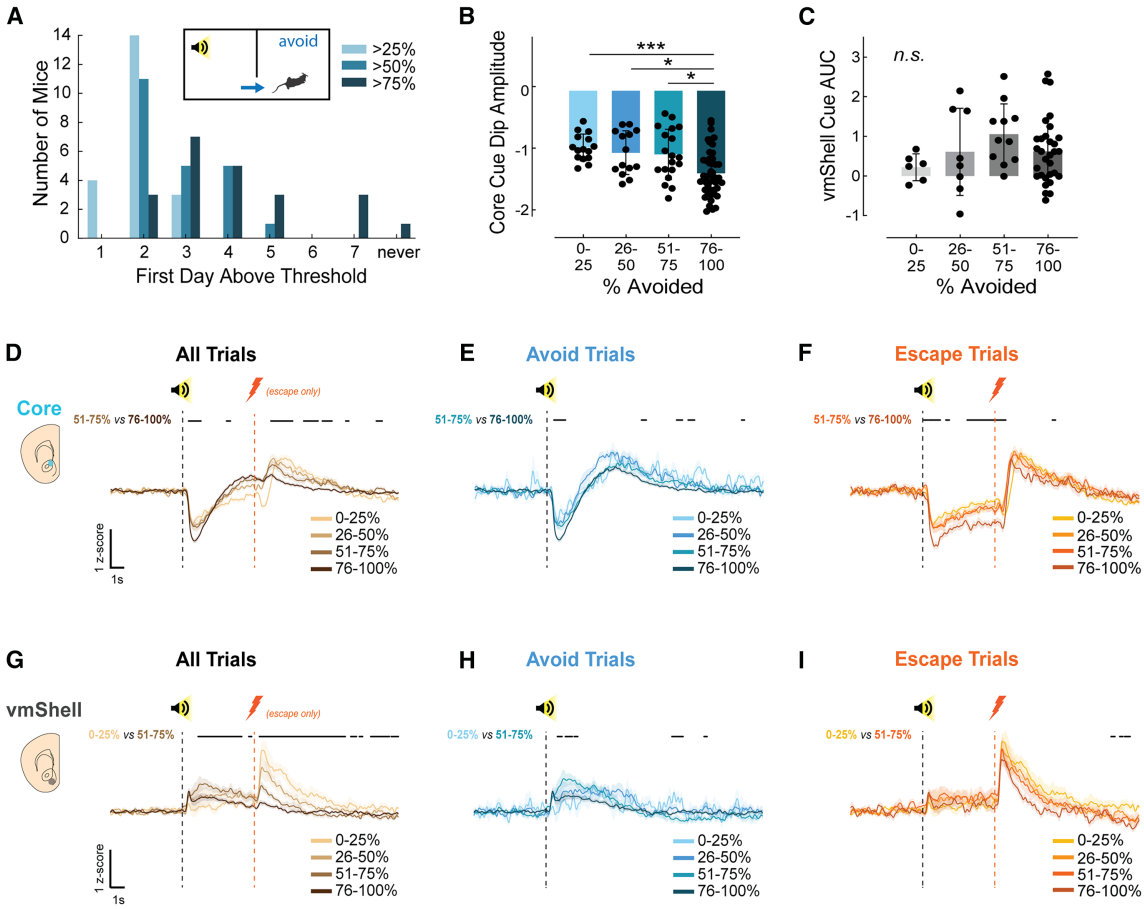

Figure 3. Core dopamine responses to the warning cue reflect consolidation of avoidance learning at high avoidance performance levels

(A) Histogram showing the number of mice reaching a threshold of performance criteria on each day. Light blue shows the number of mice reaching 25% avoidance or better for the first time on that day, medium blue shows the number of mice reaching 50% avoidance or better for the first time on that day, and dark blue shows the number of mice reaching 75% avoidance or better for the first time on that day. Although mice generally learn the avoidance task rapidly, there is individual variability in the speed of learning.

(B) Peak negative-going amplitude (cue dip amplitude) for Core by performance level. The cue dip amplitude changes minimally at lower performance levels (up to 75% avoidance) but becomes significantly larger on days with high performance (one-way ANOVA; $F_{3,\ 92} = 7.862$, $p = 0.001$; Tukey's comparisons, 0–25 versus 76–100, ***$p = 0.0009$, 26–50 versus 76–100, *$p = 0.0153$, 51–75 versus 76–100, *$p = 0.0120$). Error bars are SD.

(C) Cue area under the curve (AUC) for vmShell by performance level. Cue AUC does not significantly change due to performance (one-way ANOVA; $F_{3,\ 52} = 1.473$, $p = 0.2236$). Error bars are SD.

(D–F) Cue-aligned dopamine signals recorded from Core divided out according to the avoidance performance of the mouse rather than day recorded. For (D)–(F), significant deviations from baseline in fiber photometry signals (defined as when the bounds of the 95% CIs did not include 0) are included above each plot. The points of significance between signals for 51%–75% versus 76%–100% performance are shown as black lines above each plot (defined as when the bounds of the 95% CI did not overlap). Core dopamine dip in response to the cue was increased at 76%–100% performance regardless of trial type.

(G–I) Cue-aligned dopamine signals recorded from the vmShell divided out according to performance of the mouse rather than day recorded. For (G)–(I), significant deviations from baseline in fiber photometry signals (defined as when the bounds of the 95% CIs did not include 0) are included above each plot. The points of significance between signals for 0%–25% versus 51%–75% performance are shown as black lines above each plot (defined as when the bounds of the 95% CI did not overlap). vmShell dopamine cue responses were elevated at 51%–75% performance when analyzed by waveform analysis.

See also Figures S7 and S8.

To better understand how task-specific behavioral events predicted features of the fiber photometry data, we built linear encoding models[20–23] for each brain region and day of training to estimate temporal kernels modeling responses to cues, shocks, and crossings (Figures 2Q–2S and S5). We found that the goodness of fit for the overall model for vmShell dopamine worsened over days (slope: −0.0327, $p = 0.008$), indicating that vmShell dopamine representations of task events weaken with time (Figure 2Q). To measure the contribution of individual events to dopamine activity, we compared the fit of the full model to a reduced model with each event type removed. Using this approach, we found that the shock event contributed significantly to vmShell dopamine across all days but that the relationship was strongest on day 1 and weakened by day 3 (Figure 2R). We verified that shock encoding in the vmShell dopamine signal changed across days by modeling dopamine signal in individual mice and assessing the influence of the shock event on model performance. We found that shock representation decreased

Please cite this article in press as: Lopez et al., Region-specific nucleus accumbens dopamine signals encode distinct aspects of avoidance learning, Current Biology (2025), https://doi.org/10.1016/j.cub.2025.04.006

CellPress
OPEN ACCESS

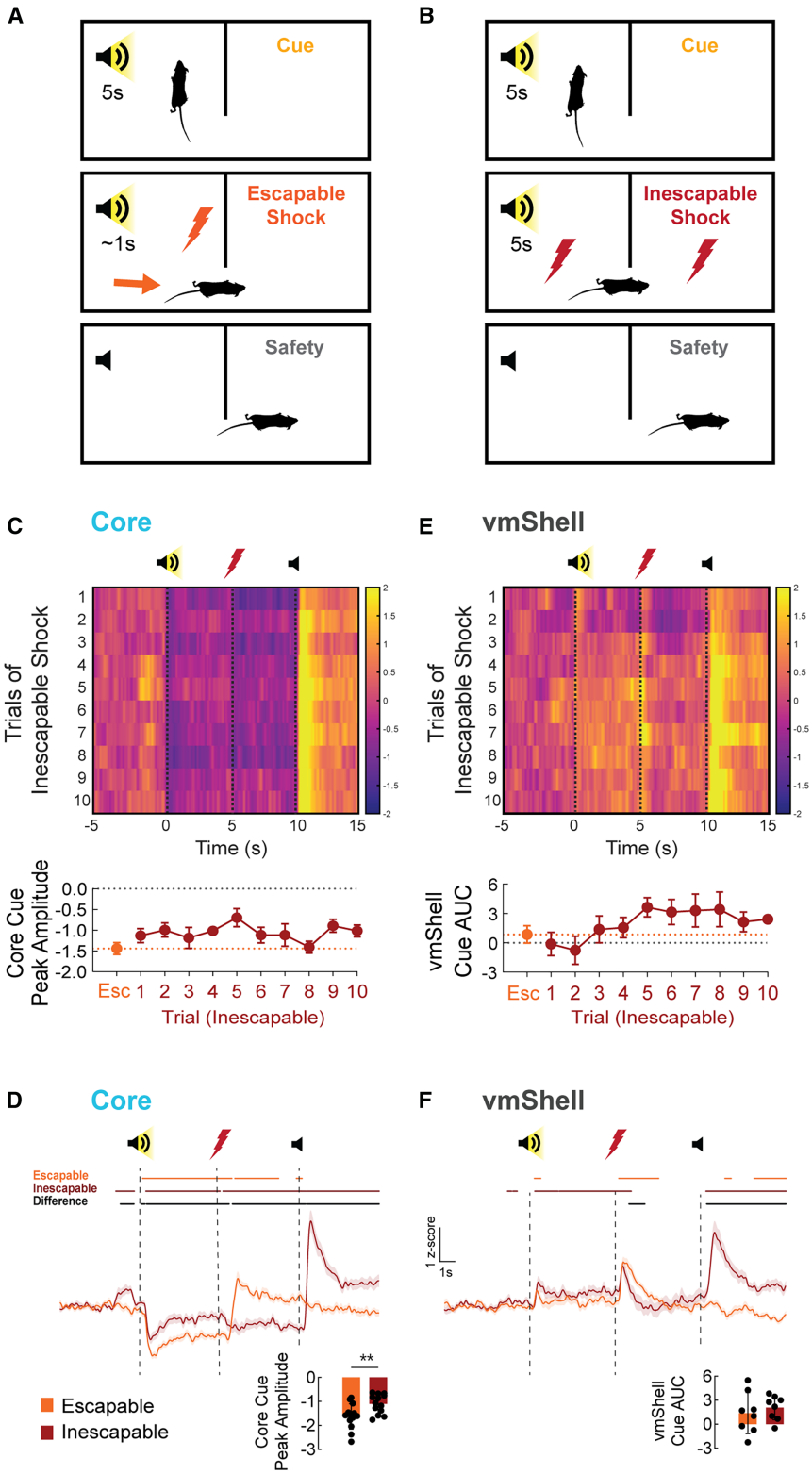

Figure 4. NAc dopamine responses to escapable shock are distinct from responses to inescapable shock

(A and B) Schematics comparing escapable and inescapable shock trials. Escapable shock trials from high-performance days (76%–100% avoidance days, when mice have learned the avoidance task well) are shown in the data below. In these trials, mice hear a 5 s warning cue, shock begins if no crossing is detected (a failed avoid trial), and mice can escape to safety in the opposite chamber. Escapable trials are contrasted by a final day of behavioral testing with 10 inescapable shock trials. In these trials, mice hear a 5 s warning cue, then experience 5 s of shock that cannot be escaped. After 5 s, the cue and shock end, and the mouse is safe for the intertrial interval period, which averages ~45 s.

(C and E) (Top) Heatmaps plotting the average dopamine signal from all mice on each of the 10 inescapable shock trials (1–10, shown descending in time) for Core (C) and vmShell (E). (Bottom) Average Core cue dip amplitude (C) or vmShell cue AUC (E) during escapable shock from high-performance days (76%–100% avoidance days, orange dots) and each of the 10 inescapable shock trials (dark red dots). Orange dotted line indicates cue dip amplitude (Core) or cue AUC (vmShell) during escapable shock from high-performance days. Error bars are SEM.

(D and F) Cue-aligned dopamine signals recorded in the Core (D) and vmShell (F) for escapable (orange) and inescapable (dark red) shock trials. The first dotted line indicates cue start, the second dotted line indicates shock start, and the third dotted line indicates shock end for inescapable shock. For (D) and (F), significant deviations from baseline in fiber photometry signals (defined as when the bounds of the 95% CIs did not include 0) are shown as orange or dark red lines for escapable or inescapable trials, respectively, above each plot. The black line indicates significant differences between escapable or inescapable plots (defined as when the bounds of the 95% CI did not overlap). (Inset) Average escapable shock cue AUCs were compared with average inescapable shock cue AUCs (average of all 10 trials). (D) Core cue peak amplitude for inescapable shocks was weakened compared with escapable shocks (paired t test, escapable versus inescapable, $t = 3.339$, $df = 12$, $^{**}p = 0.0059$). (F) VmShell cue AUC between inescapable and escapable shocks did not differ ($t = 0.9714$, $df = 7$, $p = 0.3637$). Error bars are SD.

See also Figure S9.

Please cite this article in press as: Lopez et al., Region-specific nucleus accumbens dopamine signals encode distinct aspects of avoidance learning, Current Biology (2025), https://doi.org/10.1016/j.cub.2025.04.006

across days ($F_{6,36}$ = 4.88, p = 9.64 × 10^{-4}; Figure S4). This decrease was not only due to the worsening of the full model for vmShell over time, as most representations of other events did not decrease over days.

By contrast, the overall model for Core dopamine remained strong across days (slope: −0.004, p = 0.437), with robust encoding of cues and avoidance actions (Figures 2Q and S4). The Core dopamine model showed strengthening representations of warning cues on avoid trials compared with escape trials as learning progressed, with the kernels for avoid versus escape trials diverging on days 5–7 (Figure 2S). This finding prompted us to test if decoding avoid and escape trials from Core dopamine signals during the cue period (0–3 s) on days 5–7 might also be possible. We implemented a long short-term memory fully convolutional network (LSTM-FCN),[24] which allowed us to model noisy signals without additional feature extraction or manipulation. We optimized model parameters using a Bayes optimization algorithm to maximize prediction accuracy. On test data, our decoding model achieved 87% accuracy (Figures 2T and 2U; Table S3). Analysis of the receiver operator characteristic (ROC), a common metric examining the relationship between true and false-positive rates, demonstrated an AUC (ROC-AUC) of 0.86. These results verify that the information contained within the Core dopamine signal is largely sufficient to decode established avoidance behavior on a trial-by-trial basis following learning, likely due to the divergence in the Core dopamine signal following the initial dip.

Since dopamine is associated with movement under some circumstances,[25,26] we examined the relationship between Core and vmShell dopamine signals and speed in our task (Figure S5). Overall, we found low correlations. However, in the Core, we found that correlation coefficients significantly increased, and dopamine signals became modestly correlated with crossing movements related to the task—crossing to avoid or escape. This increase in correlation between Core dopamine and speed was specific to task-related crosses and did not occur during non-meaningful ITI crossings of similar speed ($F_{1.368,\ 17.79}$ = 64.69, p < 0.0001; Figures S5A–S5D). In the vmShell, dopamine signals were significantly more correlated with speed during both task-specific and ITI crossings than during the recordings as a whole ($F_{1.454,\ 10.18}$ = 12.98, p = 0.0026; Figures S5E–S5H); however, the overall relationship remained variable and weak. We also examined whether speed was an explanatory factor in our modeling results by generating a second model that included a continuous speed regressor (Figure S6). Including speed did not substantially alter kernel values for task-related events. However, the speed contribution to the Core model grew over days and was significant on days 4–7 (Figure S6D). Together, these data suggest that Core dopamine is engaged specifically in guiding learned movements that emerge during training as instrumental responses to aversive outcomes.

Core dopamine responses to the warning cue reflect high avoidance performance

To differentiate performance from task experience, we re-analyzed our dopamine recording data by quartiles of avoidance performance (0%–25%, 26%–50%, 51%–75%, and 76%–100%). Individual mice achieve these performance levels at variable times across training (Figure 3A). We found that Core dopamine dip amplitudes increase specifically at the highest performance level of 76%–100% ($F_{3,\ 92}$ = 7.862, p = 0.001; Figure 3B). The magnitude of the Core dopamine dip in response to the cue was increased at 76%–100% performance regardless of trial type (Figures 3D–3F). Therefore, the initial magnitude of the Core dopamine dip is correlated with a consolidated understanding of task rules but does not predict trial-by-trial performance. Downstream responses in D1- and D2-SPNs in the Core also showed dynamic changes across learning (Figure S7).

By contrast, vmShell dopamine cue responses were elevated at 51%–75% performance when analyzed by waveform analysis (Figures 3G–3I) but were not significantly different by AUC analysis ($F_{3,\ 52}$ = 1.473, p = 0.2236, Figure 3C), indicating weaker effects than in Core. These data are all consistent with the idea that although cue period dopamine in the vmShell is altered during early training, it is unlikely to contribute to performance consolidation. Neither Core nor vmShell dopamine cue responses were altered according to cumulative shock experience in the task ($F_{2,93}$ = 1.642, p = 0.1991 [Core]; $F_{2,\ 53}$ = 1.574, p = 0.2168 [vmShell]; Figure S8).

NAc dopamine responses to escapable shock are distinct from responses to inescapable shock

The harms of stress to mental health are amplified by the loss of a sense of control.[27,28] The ability to learn avoidance rules can provide a sense of control, whereas poor avoidance learning could promote learned helplessness and depression.[29,30] To better understand how dopamine signals during controllable aversive stimuli would compare to an uncontrollable situation, we submitted mice to a day of inescapable shocks at the end of avoidance training. During the inescapable scenario, the same 5 s warning cue that was used during avoidance learning was followed by a 5 s footshock regardless of the animal's action (Figures 4A and 4B). We recorded Core and vmShell dopamine signals over 10 trials (Figures 4C and 4E).

We compared dopamine signals from inescapable trials to signals from escape trials performed at the 76%–100% "expert" performance level (when task rules were well understood). In Core, we observed weakened cue-related dynamics in response to inescapable shock (t = 3.339, degree of freedom [df] = 12, p = 0.0059; Figure 4D) similar in magnitude to cue-related dynamics observed in mice with low-performance (0%–25% avoidance; Figure S9A). At shock end, Core dopamine showed a large phasic increase that remained stable over trials of inescapable shock (t = 4.821, df = 12, p = 0.0004; Figures 4D and S9B).

In vmShell, cue-related dopamine dynamics, which had faded by the end of training, began to increase over trials (Figure 4E) and became statistically above baseline again by waveform analysis (Figure 4F). AUC analysis of all trials averaged, however, did not show a significant change (Figure 4F, inset). Like in the Core, the vmShell dopamine showed a large phasic increase at shock-off (t = 2.490, df = 7, p = 0.0416; Figures 4F and S9D). These data indicate that changes in NAc dopamine signals can reflect changes in avoidance rules, which is important for adapting response strategies.

DISCUSSION

We found that NAc Core and vmShell dopamine signals display different dynamics across learning during an active

avoidance (negative reinforcement) task. Core dopamine signals in response to the cue were negative-going, tracked with expert avoidance performance, and were consistent with the encoding of a safety prediction error.[3,4,14] Core dopamine signal correlations with movement were weak overall but rose during task-related instrumental responses, especially later in training, raising the intriguing possibility that Core dopamine is helping to guide learned movements. vmShell dopamine signals were positive-going, rose during early learning but faded later, and were consistent with the encoding of aversive salience.[31,32] Our data illustrate how Core and vmShell dopamine signals vary by subregion and how their computations relate to learned behavioral strategies as mice transition from naive to expert avoidance. Our work supports a model for Core and vmShell dopamine function in which these regions not only encode aversion oppositely in Pavlovian settings but also guide avoidance through different computational principles. Further understanding computational heterogeneity in dopamine function and its behavioral consequences can provide avenues to understand how dopamine subpopulations work in concert to provide animals with tools to avoid danger in their environment.

Our data agree with previous work reporting that Core dopamine decreases and vmShell dopamine increases for shocks and shock-predicting cues,[3,6–8,13,14] confirming that this heterogeneity in response to aversive stimuli relates strongly to anatomy. Although numerous studies have detected positive-going dopamine signals in response to aversive events,[1–4] debate continues about the specific locations where these responses occur. Efforts to identify variables contributing to discrepancies across labs (e.g., subtle differences in mouse versus rat NAc subregion boundaries or anterior-posterior coordinates) would help the field coalesce. Agreement in defining anatomical subregions could be aided by the discovery of reliable molecular markers for projection-targeted dopamine neurons directly related to physiological function.

By employing a final day of inescapable shocks after successful avoidance learning, we showed how the controllability of the shock influences NAc dopamine. Notably, the cessation of the inescapable shock evoked large phasic dopamine transients across NAc subregions. Previous research has shown that ventral tegmental area (VTA) dopamine neuron responses at shock termination are important for motivated behavior to escape shocks and can be diminished by learned helplessness.[33] However, it remains unclear whether there is any important regional variation of dopamine signals and the information they encode at shock termination. Further research to understand these shock-termination signals, how they are generated, and how they might vary in rodent models of anxiety, depression, and OCD would be revealing.

RESOURCE AVAILABILITY

Lead contact

Further information and requests for resources and reagents should be directed to and will be fulfilled by the lead contact, Talia Lerner (talia.lerner@northwestern.edu).

Materials availability

This study did not generate new unique reagents.

Data and code availability

- All data reported in this paper will be shared by the lead contact upon request. Data will be deposited in the DANDI archive and publicly available as of the date of publication.
- All original code for fiber photometry analysis has been deposited to Github and is publicly available as of the date of publication. DOIs are listed in the key resources table.
- Any additional information required to reanalyze the data reported in this paper is available from the lead contact upon request.

ACKNOWLEDGMENTS

We thank the Lerner laboratory for helpful discussions and critical feedback throughout the project. We thank the Center for Comparative Medicine at Northwestern University for providing animal care and husbandry. We thank the members of the Center for Translational Pain Research, particularly Drs. Vania Apkarian, Marco Martina, and Jones Parker, for input, feedback, and support on these studies. This work was supported by the National Institutes of Health (P50DA044121, R00MH109569, and DP2MH122401 to T.N.L.; F31DA056200 to G.C.L.; and F32DK135313 to M.D.S.). J.M.C. was supported by a NARSAD Young Investigator Grant from the Brain and Behavior Research Foundation, a Whitehall Foundation Research Grant, and a Shaw Family Pioneer Award from the Center for Reproductive Science at Northwestern University.

AUTHOR CONTRIBUTIONS

G.C.L. and T.N.L. conceived the experiments, and G.C.L. and L.D.V.C. executed them. G.C.L., L.D.V.C., R.F.K., M.D.S., J.M.C., V.N.S., and T.N.L. analyzed the data, including modeling studies. J.M.C. and T.N.L. provided oversight and support for the project. G.C.L. and T.N.L. wrote the manuscript with assistance from the other authors.

DECLARATION OF INTERESTS

The authors declare no competing interests.

STAR★METHODS

Detailed methods are provided in the online version of this paper and include the following:

- KEY RESOURCES TABLE
- EXPERIMENTAL MODEL AND STUDY PARTICIPANT DETAILS
- METHOD DETAILS
  - Surgery
  - Behavior
  - Video Analysis
  - Fiber photometry
  - Perfusions and histology
  - Exclusions
- QUANTIFICATION AND STATISTICAL ANALYSIS
  - Behavioral analysis
  - Fiber photometry signal processing and analysis
  - Encoding model of dopamine fluorescence
  - Deep Learning Classification Decoder
  - Other statistical methods

SUPPLEMENTAL INFORMATION

Supplemental information can be found online at https://doi.org/10.1016/j.cub.2025.04.006.

Received: September 6, 2024
Revised: February 14, 2025
Accepted: April 2, 2025
Published: April 22, 2025

REFERENCES

1. Matsumoto, M., and Hikosaka, O. (2009). Two types of dopamine neuron distinctly convey positive and negative motivational signals. Nature *459*, 837–841. https://doi.org/10.1038/nature08028.
2. Brischoux, F., Chakraborty, S., Brierley, D.I., and Ungless, M.A. (2009). Phasic excitation of dopamine neurons in ventral VTA by noxious stimuli. Proc. Natl. Acad. Sci. USA *106*, 4894–4899. https://doi.org/10.1073/pnas.0811507106.
3. Yuan, L., Dou, Y.-N., and Sun, Y.-G. (2019). Topography of Reward and Aversion Encoding in the Mesolimbic Dopaminergic System. J. Neurosci. *39*, 6472–6481. https://doi.org/10.1523/JNEUROSCI.0271-19.2019.
4. Lerner, T.N., Shilyansky, C., Davidson, T.J., Evans, K.E., Beier, K.T., Zalocusky, K.A., Crow, A.K., Malenka, R.C., Luo, L., Tomer, R., et al. (2015). Intact-Brain Analyses Reveal Distinct Information Carried by SNc Dopamine Subcircuits. Cell *162*, 635–647. https://doi.org/10.1016/j.cell.2015.07.014.
5. Verharen, J.P.H., Zhu, Y., and Lammel, S. (2020). Aversion hot spots in the dopamine system. Curr. Opin. Neurobiol. *64*, 46–52. https://doi.org/10.1016/j.conb.2020.02.002.
6. de Jong, J.W., Afjei, S.A., Pollak Dorocic, I., Peck, J.R., Liu, C., Kim, C.K., Tian, L., Deisseroth, K., and Lammel, S. (2019). A Neural Circuit Mechanism for Encoding Aversive Stimuli in the Mesolimbic Dopamine System. Neuron *101*, 133–151.e7. https://doi.org/10.1016/j.neuron.2018.11.005.
7. Salinas-Hernández, X.I., Zafiri, D., Sigurdsson, T., and Duvarci, S. (2023). Functional architecture of dopamine neurons driving fear extinction learning. Neuron *111*, 3854–3870.e5. https://doi.org/10.1016/j.neuron.2023.08.025.
8. Badrinarayan, A., Wescott, S.A., Vander Weele, C.M.V., Saunders, B.T., Couturier, B.E., Maren, S., and Aragona, B.J. (2012). Aversive Stimuli Differentially Modulate Real-Time Dopamine Transmission Dynamics within the Nucleus Accumbens Core and Shell. J. Neurosci. *32*, 15779–15790. https://doi.org/10.1523/JNEUROSCI.3557-12.2012.
9. Hofmann, S.G., and Hay, A.C. (2018). Rethinking Avoidance: Toward a Balanced Approach to Avoidance in Treating Anxiety Disorders. J. Anxiety Disord. *55*, 14–21. https://doi.org/10.1016/j.janxdis.2018.03.004.
10. Ball, T.M., and Gunaydin, L.A. (2022). Measuring maladaptive avoidance: from animal models to clinical anxiety. Neuropsychopharmacology *47*, 978–986. https://doi.org/10.1038/s41386-021-01263-4.
11. Wise, R.A. (2004). Dopamine, learning and motivation. Nat. Rev. Neurosci. *5*, 483–494. https://doi.org/10.1038/nrn1406.
12. Schultz, W., Dayan, P., and Montague, P.R. (1997). A neural substrate of prediction and reward. Science *275*, 1593–1599. https://doi.org/10.1126/science.275.5306.1593.
13. Oleson, E.B., Gentry, R.N., Chioma, V.C., and Cheer, J.F. (2012). Subsecond Dopamine Release in the Nucleus Accumbens Predicts Conditioned Punishment and Its Successful Avoidance. J. Neurosci. *32*, 14804–14808. https://doi.org/10.1523/JNEUROSCI.3087-12.2012.
14. Stelly, C.E., Haug, G.C., Fonzi, K.M., Garcia, M.A., Tritley, S.C., Magnon, A.P., Ramos, M.A.P., and Wanat, M.J. (2019). Pattern of dopamine signaling during aversive events predicts active avoidance learning. Proc. Natl. Acad. Sci. USA *116*, 13641–13650. https://doi.org/10.1073/pnas.1904249116.
15. Chou, S.-H., Chen, Y.-J., Liao, C.-P., and Pan, C.-L. (2022). A role for dopamine in *C. elegans* avoidance behavior induced by mitochondrial stress. Neurosci. Res. *178*, 87–92. https://doi.org/10.1016/j.neures.2022.01.005.
16. Akiti, K., Tsutsui-Kimura, I., Xie, Y., Mathis, A., Markowitz, J.E., Anyoha, R., Datta, S.R., Mathis, M.W., Uchida, N., and Watabe-Uchida, M. (2022). Striatal dopamine explains novelty-induced behavioral dynamics and individual variability in threat prediction. Neuron *110*, 3789–3804.e9. https://doi.org/10.1016/j.neuron.2022.08.022.
17. Wenzel, J.M., Oleson, E.B., Gove, W.N., Cole, A.B., Gyawali, U., Dantrassy, H.M., Bluett, R.J., Dryanovski, D.I., Stuber, G.D., Deisseroth, K., et al. (2018). Phasic Dopamine Signals in the Nucleus Accumbens that Cause Active Avoidance Require Endocannabinoid Mobilization in the Midbrain. Curr. Biol. *28*, 1392–1404.e5. https://doi.org/10.1016/j.cub.2018.03.037.
18. Hollon, N.G., Soden, M.E., and Wanat, M.J. (2013). Dopaminergic Prediction Errors Persevere in the Nucleus Accumbens Core during Negative Reinforcement. J. Neurosci. *33*, 3253–3255. https://doi.org/10.1523/JNEUROSCI.5762-12.2013.
19. Sherathiya, V.N., Schaid, M.D., Seiler, J.L., Lopez, G.C., and Lerner, T.N. (2021). GuPPy, a Python toolbox for the analysis of fiber photometry data. Sci. Rep. *11*, 24212. https://doi.org/10.1038/s41598-021-03626-9.
20. Cox, J., Minerva, A.R., Fleming, W.T., Zimmerman, C.A., Hayes, C., Zorowitz, S., Bandi, A., Ornelas, S., McMannon, B., Parker, N.F., et al. (2023). A neural substrate of sex-dependent modulation of motivation. Nat. Neurosci. *26*, 274–284. https://doi.org/10.1038/s41593-022-01229-9.
21. Engelhard, B., Finkelstein, J., Cox, J., Fleming, W., Jang, H.J., Ornelas, S., Koay, S.A., Thiberge, S.Y., Daw, N.D., Tank, D.W., et al. (2019). Specialized coding of sensory, motor and cognitive variables in VTA dopamine neurons. Nature *570*, 509–513. https://doi.org/10.1038/s41586-019-1261-9.
22. Choi, J.Y., Jang, H.J., Ornelas, S., Fleming, W.T., Fürth, D., Au, J., Bandi, A., Engel, E.A., and Witten, I.B. (2020). A Comparison of Dopaminergic and Cholinergic Populations Reveals Unique Contributions of VTA Dopamine Neurons to Short-Term Memory. Cell Rep. *33*, 108492. https://doi.org/10.1016/j.celrep.2020.108492.
23. Pinto, L., and Dan, Y. (2015). Cell-Type-Specific Activity in Prefrontal Cortex during Goal-Directed Behavior. Neuron *87*, 437–450. https://doi.org/10.1016/j.neuron.2015.06.021.
24. Karim, F., Majumdar, S., Darabi, H., and Harford, S. (2019). Multivariate LSTM-FCNs for Time Series Classification. Neural Netw. *116*, 237–245. https://doi.org/10.1016/j.neunet.2019.04.014.
25. Azcorra, M., Gaertner, Z., Davidson, C., He, Q., Kim, H., Nagappan, S., Hayes, C.K., Ramakrishnan, C., Fenno, L., Kim, Y.S., et al. (2023). Unique functional responses differentially map onto genetic subtypes of dopamine neurons. Nat. Neurosci. *26*, 1762–1774. https://doi.org/10.1038/s41593-023-01401-9.
26. Coddington, L.T., and Dudman, J.T. (2019). Learning from Action: Reconsidering Movement Signaling in Midbrain Dopamine Neuron Activity. Neuron *104*, 63–77. https://doi.org/10.1016/j.neuron.2019.08.036.
27. Riachi, E., Holma, J., and Laitila, A. (2024). Psychotherapists' perspectives on loss of sense of control. Brain Behav. *14*, e3368. https://doi.org/10.1002/brb3.3368.
28. Hancock, L., and Bryant, R.A. (2020). Posttraumatic stress, stressor controllability, and avoidance. Behav. Res. Ther. *128*, 103591. https://doi.org/10.1016/j.brat.2020.103591.
29. Chase, H.W., Frank, M.J., Michael, A., Bullmore, E.T., Sahakian, B.J., and Robbins, T.W. (2010). Approach and avoidance learning in patients with major depression and healthy controls: relation to anhedonia. Psychol. Med. *40*, 433–440. https://doi.org/10.1017/S0033291709990468.
30. Grant, D.M., Wingate, L.R., Rasmussen, K.A., Davidson, C.L., Slish, M.L., Rhoades-Kerswill, S., Mills, A.C., and Judah, M.R. (2013). An Examination of the Reciprocal Relationship Between Avoidance Coping and Symptoms of Anxiety and Depression. J. Soc. Clin. Psychol. *32*, 878–896. https://doi.org/10.1521/jscp.2013.32.8.878.
31. Kutlu, M.G., Zachry, J.E., Melugin, P.R., Cajigas, S.A., Chevee, M.F., Kelly, S.J., Kutlu, B., Tian, L., Siciliano, C.A., and Calipari, E.S. (2021). Dopamine release in the nucleus accumbens core signals perceived saliency. Curr. Biol. *31*, 4748–4761.e8. https://doi.org/10.1016/j.cub.2021.08.052.
32. Lopez, G.C., and Lerner, T.N. (2025). How dopamine enables learning from aversion. Curr. Opin. Behav. Sci. *61*, 101476. https://doi.org/10.1016/j.cobeha.2024.101476.

33. Wu, M., Minkowicz, S., Dumrongprechachan, V., Hamilton, P., Xiao, L., and Kozorovitskiy, Y. (2021). Attenuated dopamine signaling after aversive learning is restored by ketamine to rescue escape actions. eLife *10*, e64041. https://doi.org/10.7554/eLife.64041.

34. Pereira, T.D., Tabris, N., Matsliah, A., Turner, D.M., Li, J., Ravindranath, S., Papadoyannis, E.S., Normand, E., Deutsch, D.S., Wang, Z.Y., et al. (2022). SLEAP: A deep learning system for multi-animal pose tracking. Nat. Methods *19*, 486–495. https://doi.org/10.1038/s41592-022-01426-1.

35. Goodwin, N.L., Choong, J.J., Hwang, S., Pitts, K., Bloom, L., Islam, A., Zhang, Y.Y., Szelenyi, E.R., Tong, X., Newman, E.L., et al. (2024). Simple Behavioral Analysis (SimBA) as a platform for explainable machine learning in behavioral neuroscience. Nat. Neurosci. *27*, 1411–1424. https://doi.org/10.1038/s41593-024-01649-9.

36. Jean-Richard-dit-Bressel, P., Clifford, C.W.G., and McNally, G.P. (2020). Analyzing Event-Related Transients: Confidence Intervals, Permutation Tests, and Consecutive Thresholds. Front. Mol. Neurosci. *13*, 14. https://doi.org/10.3389/fnmol.2020.00014.

37. Ramsay, J.O. (2003). Matlab, R and S-PLUS Functions for Functional Data Analysis. https://www.psych.mcgill.ca/misc/fda/downloads/FDAfuns/R/inst/Matlab/fdaM/FDAfuns.pdf.

38. Wu, J., Chen, X.-Y., Zhang, H., Xiong, L.-D., Lei, H., and Deng, S.-H. (2019). Hyperparameter Optimization for Machine Learning Models Based on Bayesian Optimizationb. J. Electron. Sci. Technol. *17*, 26–40. https://doi.org/10.11989/JEST.1674-862X.80904120.

39. Comet.ml (2024). Supercharging Machine Learning. https://www.comet.com/mschaid/lstmnfcn-bayes-tuning-5-day-weighted/view/new/panels.

Please cite this article in press as: Lopez et al., Region-specific nucleus accumbens dopamine signals encode distinct aspects of avoidance learning, Current Biology (2025), https://doi.org/10.1016/j.cub.2025.04.006

STAR★METHODS

KEY RESOURCES TABLE

REAGENT or RESOURCE	SOURCE	IDENTIFIER
Antibodies		
Rabbit anti-GFP	Invitrogen	Cat# A11122; RRID: AB_221569
Donkey anti-Rabbit Alexa Fluor 647	Jackson ImmunoResearch	Cat# 711-606-152; RRID: AB_2492288
Bacterial and virus strains		
AAV9-CAG-dLight1.3b	Virovek	Lot# 19-508
AAV1-CAG-FLEX-NES-jRCaMP1b	Addgene	Lot# CS1187; RRID: Addgene_100849
Chemicals, peptides, and recombinant proteins		
Isoflurane	Henry Schein	N/A
Meloxicam	Covetrus	N/A
Bupivacaine	Hospira	N/A
Euthasol	Virbac	N/A
Normal Goat Serum	Jackson ImmunoResearch Laboratories	Lot#153636; RRID: AB_2336990
DAPI Fluoromount-G	Southern Biotech	Cat# 0100-20
Triton-X	Sigma	Cat#X100-1L
Deposited data		
Data Analysis Code (MATLAB)	Generated by study	GitHub: https://github.com/glopez924/Lopez-et-al-2025.git
Experimental models: Organisms/strains		
Mouse: Wildtype C57BL6/J	Jackson Laboratory	Strain #:000664; RRID:IMSR_JAX:000664
Mouse: Tg(Drd1-Cre)FK150Gsat	GENSAT	RRID: MMRRC_036916-UCD
Mouse: Tg(Adora2a-Cre)KG139Gsat	GENSAT	RRID:MMRRC_036158-UCD
Software and algorithms		
GuPPy	Lerner Lab	https://github.com/LernerLab/GuPPy/wiki; RRID: SCR_022353
Synapse	Tucker Davis Technologies	https://www.tdt.com/component/synapsesoftware/; RRID: SCR_024878
MED-PC V	Med Associates	https://www.med-associates.com/medpc-v/; RRID: SCR_012156
MATLAB	Mathworks	https://www.mathworks.com/products/ matlab.html; RRID: SCR_001622
SLEAP	Murthy Lab	https://github.com/talmolab/sleap; RRID: SCR_021382
SimBA	Golden Lab	https://github.com/sgoldenlab/simba; RRID:SCR_021413

EXPERIMENTAL MODEL AND STUDY PARTICIPANT DETAILS

Adult female and male mice were group-housed by sex under a reverse 12:12 h light/dark cycle. All mice were given ad libitum access to food and water. Experiments were performed during the dark cycle. Wildtype C57BL6/J mice (Jackson Strain #:000664) were used for vmShell experiments. Heterozygous Tg(Drd1-Cre)FK150Gsat and Tg(Adora2a-Cre)KG139Gsat mice, generated by crossing homozygous Tg(Drd1-Cre)FK150Gsat or Tg(Adora2a-cre)KG139Gsat mice with WT (C57BL6/J) in-house, were used for Core experiments to allow for recording of calcium activity in D1- and D2-spiny projection neurons, respectively, for an additional downstream circuit experiment (Figure S6). No differences in avoidance behavior by genotype were observed (Figure S6B). Littermates were randomly assigned to experimental groups (Core: 5 females, 9 males; vmShell: 5 females, 3 males). All experiments were approved by the Northwestern University Institutional Animal Care and Use Committee.

Please cite this article in press as: Lopez et al., Region-specific nucleus accumbens dopamine signals encode distinct aspects of avoidance learning, Current Biology (2025), https://doi.org/10.1016/j.cub.2025.04.006

CellPress
OPEN ACCESS

METHOD DETAILS

Surgery

Viral injection and optic fiber implant surgeries were performed on adult mice at 7-10 weeks of age. Mice were anesthetized in an isoflurane chamber at 3-4% isoflurane (Henry Schein) and then placed on a stereotaxic frame (Stoelting). Anesthesia was maintained at 1-3% isoflurane. Mice were injected with meloxicam (Covetrus, 20 mg/kg) subcutaneously prior to the start of surgery to minimize post-surgical pain. Hair was removed from the top of the head using Nair. The exposed skin was disinfected with alcohol and a povidone-iodine solution. Prior to incision, bupivacaine (Hospira, 2 mg/kg) was injected subcutaneously at the incision site. The scalp was opened using a sterile scalpel and holes were drilled in the skull at the appropriate stereotaxic coordinates. Viruses were infused at 100 nL/min through a blunt 33-gauge injection needle using a syringe pump (World Precision Instruments). The needle was left in place for 5 min following the end of the injection, then slowly retracted to avoid leakage up the injection tract. Implants were secured to the skull with Metabond (Parkell) and Flow-it ALC blue light-curing dental epoxy (Pentron). After surgery, mice were allowed to recover until ambulatory on a heated pad, then returned to their homecage with moistened chow or DietGel available. The mice were checked after 24 hours and provided with another dose of meloxicam. Mice then recovered for three to four weeks before behavioral experiments began.

A2A-Cre and D1-Cre mice were injected with a 500 nL virus cocktail containing AAV9-CAG-dLight1.3b (1.25e12 vg/ml, Virovek) and AAV1-CAG-FLEX-NES-jRCaMP1b (2.6e12 vg/ml, Addgene) into the Core (AP 1.5, ML 0.9, DV -4.1) in one hemisphere. Hemispheres were counterbalanced between mice. Fiber optic implants (Doric Lenses; 400 μm, 0.48 NA, 1.25 mm ferrules) were placed above the Core (AP 1.5 mm, ML 0.9 mm, DV -4.0 mm) in the same injection hemisphere. WT mice were injected with 500 nL of AAV9-CAG-dLight1.3b (1.25e12 vg/ml, Virovek) into the vmShell (AP 1.5, ML 0.6, DV -4.8) in one hemisphere. Hemispheres were counterbalanced between mice. Fiber optic implants (Doric Lenses; 200 μm, 0.48 NA, 1.25 mm ferrules) were placed above the vmShell (AP 1.5 mm, ML 0.6 mm, DV -4.7 mm) in the same injection hemisphere.

Behavior

Mice underwent two shock-paired behavioral paradigms sequentially: active avoidance, then inescapable shock. Both tests were completed using custom 2-chamber shuttle boxes, with chambers separated by a plastic door (MED Associates). The day before testing began, mice were habituated to tethering with patch cords (Doric Lenses) in an open field chamber for 5 minutes. During active avoidance, mice were tethered with patch cords and then placed in either the right or left shuttle box chamber initially chosen randomly and alternating starting side each day. Once a mouse was detected in a chamber, a sound (2900 Hz tone) and white light (40 lux) cue turned on for 5 s coincident with the door connecting the two chambers opening. If the mouse shuttled from its initial chamber to the opposite chamber within 5 s, the light and sound cue turned off and no shock was delivered (“avoid” trial). If the mouse failed to cross over to the opposite chamber within 5 s, a 0.4 mA shock turned on and continued for 25 s or until the mouse shuttled to the opposite chamber. Shuttling during the shock also terminated the light and sound cues ending the trial (“escape” trial). Random length intertrial intervals ranging from 30 s to 60 s (45 s average) separated each trial. (Figure 1C). There were no failed trials in this task – mice reliably escaped shortly after the shock began (~1 sec post-shock). Mice were tested on this task for 7 days, 30 trials per day. After active avoidance testing, mice underwent one day of inescapable shock. For this task, mice were tethered and placed within the 2-chamber shuttle box as previously described. Once a mouse was detected in a chamber the door separating the chambers was retracted accompanied by a sound and light cue that persisted for 5 s. After 5 s, a 0.4 mA shock turned on and remained on for 5 s. Mice were able to shuttle between chambers, but this behavior did not prevent or stop the shock. After 5 s, the shock and cues turned off. Mice were tested on this task for 1 session consisting of 10 trials.

Video Analysis

Mouse pose estimation was conducted using SLEAP.[34] Body part points (nose, left ear, right ear, mid-body, left body, right body, and tail base) were manually placed on sample video frames to train a model to accurately predict body part locations. One to two hundred labels were added at a time to generate intermediate models and assess accuracy. Ultimately, 679 frames across all videos were labeled to achieve human-like labeling accuracy with minimal artifacts. The top 1% of predicted movements (corresponding to those > 480cm/s) were removed as artifacts largely stemming from frames where the mouse was not detected by SLEAP. Nose and mid-body points generated from the SLEAP model were then used for behavioral classification of freezing and side crossing, respectively, using Simple Behavior analysis (SimBA) software.[35] Speed of the nose was used to determine freezing, defined as <0.22cm/frame (6.6cm/s) movements for at least 2s in R. For side crossing timestamp extraction, ROIs were custom fit using SimBA in each video to indicate different sides of the behavioral apparatus and the time at which the mid-body point traversed the ROI side boundary was used and aligned to photometry data in R.

Fiber photometry

All recordings were performed using a fiber photometry rig with optical components from Doric lenses and Tucker Davis Technologies (TDT) controlled by a real-time processor from TDT (RZ5P or RZ10X). TDT Synapse software was used for data acquisition. 465nm, 405nm, and 560nm LEDs were modulated at 210 Hz, 330 Hz, and 450 Hz, respectively, for Core A2A- and D1-Cre probes. 465nm and 405nm LEDs were modulated at 210 Hz and 330 Hz, respectively for vmShell experiments. LED currents were adjusted to return a voltage between 150-200mV for each signal, were offset by 5 mA, were demodulated using a 4 Hz lowpass frequency filter.

Please cite this article in press as: Lopez et al., Region-specific nucleus accumbens dopamine signals encode distinct aspects of avoidance learning, Current Biology (2025), https://doi.org/10.1016/j.cub.2025.04.006

Behavioral timestamps, e.g., for cue and shuttle crossings, were fed into the real-time processor as TTL signals from the shuttle boxes (MED Associates) for alignment with the neural data. GuPPy, an opensource Python-based photometry data analysis pipeline, was used to process fiber photometry data and align signals to specific time-locked events.[19]

Perfusions and histology

Mice received lethal i.p. injections of Euthasol (Virbac, 1mg/kg) to induce a rapid onset of unconsciousness and death. Once unresponsive to a firm toe pinch, an incision was made up the middle of the body cavity. An injection needle was inserted into the left ventricle of the heart, the right atrium was punctured, and solution (PBS followed by 4% PFA) was infused into the left ventricle as the mouse was exsanguinated. The mouse was then decapitated, and its brain was removed and fixed overnight at 4°C in 4% PFA. After perfusion and fixation, brains were transferred to a solution of 30% sucrose in PBS (w/v), where they were stored for at least two overnights at 4°C before sectioning. Tissue was sectioned on a freezing microtome (Leica) at 30 μm, stored in cryoprotectant (30% sucrose, 30% ethylene glycol, 1% polyvinyl pyrrolidone in PB) at 4°C until immunostaining.

Anti-GFP staining was performed on free floating sections to amplify signals from dLight1.3b. Sections were blocked in 3% normal goat serum in PBS for 1 h at room temperature. Primary antibody staining was performed using 1:500 Rabbit anti-GFP primary antibody (Invitrogen, A11122) in blocking solution at 4°C for 48 hrs. Secondary staining was performed using 1:500 donkey anti-rabbit Alexa Fluor 647 (Jackson ImmunoResearch, 711-606-152) in blocking solution at room temperature for 2 hrs. Tissue was mounted on slides in PBS and coverslips (Fisherbrand, Cat. No. 1255005) mounted with DAPI Fluoromont-G (Southern Biotech). Slides were imaged using a fluorescent microscope (Keyence BZ-X710) with 5x, 10x, and 40x air immersion objectives. Probe placements were determined by comparing their location to the Allen Mouse Brain Atlas.

Exclusions

One mouse was excluded from the Core experiments due to failure to reach more than 40% avoidance after 7 days of active avoidance testing. Four mice were eliminated due to poor photometry signal, reflected by poor dLight1.3b expression in histology. All n values listed above do not include these mice.

QUANTIFICATION AND STATISTICAL ANALYSIS

Behavioral analysis

Behavioral data such as number of avoided or escaped trials and latencies to cross were collected automatically by MED-PC software (Med Associates; Figures 1D and 1E). Percent avoidance was calculated by taking the number of avoided trials and dividing it by the total number of trials in the task (30 trials), then multiplying by 100 (Figure 1D). Percent time frozen, speed, and inter-trial interval (ITI) crossing data were extracted via SLEAP[34] for animal pose tracking and SimBA[35] for behavioral classification (Figures 1F, 1G, S2, S3, and S5).

Fiber photometry signal processing and analysis

GuPPy[19] was used to analyze dLight1.3b and jRCaMP1b signals time-locked to specific behavioral events using default settings. In brief, raw data were passed through a zero-phase digital filter and a least-squares linear fit was applied to the 405nm control signal to align it to the 465nm or 560nm signal. ΔF/F was calculated with the following formula: (signal - fitted control) / (fitted control). To facilitate comparisons across animals, z-scores were calculated by subtracting the mean ΔF/F calculated across the entire session and dividing by the standard deviation (GuPPy standard z-score method; See Figure S1). Peristimulus time-histogram (PSTH) parameters were set from -25 to 20 seconds and baseline parameters were set to from -5 to -2 seconds. H5 output files from GuPPy were imported into MATLAB for further quantitative analysis. Area-under-the-curve (AUC) was calculated in MATLAB using the trapz function, with positive and negative values indicating that the AUC is above or below zero, respectively. Dip amplitudes were calculated in MATLAB by inverting the plots about the y-axis and using the max and findpeaks functions (n = 22, Figures 1, 2, 3, 4, S3, S7, and S9). Correlations between movement and photometry data were calculated in MATLAB using the corrcoef function (Figure S5). Bootstrapped confidence interval (bCI) waveform analyses (95% CI) were conducted to identify significant deviations from baseline in fiber photometry signals (defined as when the bounds of the 95% CIs did not include 0) and to determine when Core and vmShell signals differed (defined as when the bounds of the 95% CI did not overlap) via an adapted MATLAB script as described by Jean-Richard-dit-Bressel et al. (n = 22, Figures 1, 2, 3, 4, and S8).[36] We applied consecutive thresholds to the bCI analyses using the full length of the low-pass filter window. The consecutive threshold was determined by dividing the sampling rate of our signal (1017.25 Hz) by the critical frequency (defined as sampling rate/(2*moving average filter window)). This gave us a consecutive threshold of ∼200 data points such that the bCI waveform analyses identified significant deviations only when the bounds of the 95% CIs did not include 0 or did not overlap for more than 200 consecutive data points.

Encoding model of dopamine fluorescence

To relate dopamine activity to behavioral events while accounting for the linear contributions of other events occurring close in time, we built a kernel-based encoding model of the photometry signals. For each session, we first downsampled the photometry traces to 20 Hz and then concatenated the photometry data across mice. We then used a multiple linear regression analysis with the photometry signal as the dependent variable and behavioral events as independent variables. To account for lags in the relationship between

Please cite this article in press as: Lopez et al., Region-specific nucleus accumbens dopamine signals encode distinct aspects of avoidance learning, Current Biology (2025), https://doi.org/10.1016/j.cub.2025.04.006

changes in fluorescence and behavioral events, we generated the independent variables by convolving a spline basis set with a binary vector of event times (1 at the time of the event, 0 otherwise). The spline basis set was generated with the MATLAB package fDAm.[37] The full model is:

$$F(t) = \beta_0 + \sum_{i=1}^{n_{events}} \sum_{j=1}^{n_{dof}} \beta_{ij} S_j(t) * c_i(t) + \epsilon .$$

$F(t)$ is the z-scored ΔF/F at time t, β_0 is the intercept, ϵ is the error, n_{events} is the number of events, β_{ij} is the regression coefficient for the jth basis function, S_j, for event i, n_{dof} is the number of degrees of freedom of the basis set and $\boldsymbol{c}_i$ is a binary vector that is the same length as F and is 1 at the time of event i and 0 otherwise. ΔF/F is modeled as the convolution of the event vector, $\boldsymbol{c}_i$, with a temporal kernel K_i, summed across events:

$$F(t) = \beta_0 + \sum_{i=1}^{n_{events}} K_t(t) * c_i(t) + \epsilon.$$

The temporal kernel for event i is defined as

$$K_i(t) = \sum_{j=1}^{n_{dof}} \beta_{ij} S_j(t).$$

We estimated temporal kernels for the cue and cross events separately for trials when the mouse avoided or escaped the shock, the escape and avoid cross events, and the shock presentation. Temporal kernels for the cue events spanned from 2 seconds before to 1.5 seconds after the event, the shock kernel spanned from 0.5 seconds before to 1.5 seconds after the event, the avoid cross kernel spanned from 1 second before to 5 seconds after the event and the escape cross kernel spanned from 0 seconds to 5 seconds after the event. The degrees of freedom for the basis set was dependent on the duration of the event. Basis sets for cue events had 25 degrees of freedom, shock 14, avoid crosses 42 and escape crosses 35. We estimated these kernels with linear regression with lasso regularization using the MATLAB function lasso. We first selected a regularization parameter, λ. Using 5-fold cross validation, we fit the model using a range of λ values. We selected the value of λ that minimized the mean squared error calculated with the test data set (~20% of trials in each cross-validation partition) in each partition and used the average to fit the full data set.

Model performance was assessed by computing the correlation coefficient between the real ΔF/F and the ΔF/F estimated with the model. To estimate confidence intervals, we bootstrapped the dataset by trial 5000 times to obtain a distribution of model fits. To assess the change in goodness of fit across days (Figure 2Q), we fit a line to the median of the bootstrapped correlation coefficients by day. To quantify the contribution of the shock event to the model fit (Figure 2R), we fit a second model to the data with the shock predictors removed and then computed the difference in fit (correlation coefficients) for the full model and the reduced model. The removal of the shock event was considered significant if the confidence interval of the difference did not contain 0 (alpha = 0.05 with a Bonferroni correction for multiple comparisons). To compare the amplitude of the response to the cue preceding shock avoidance and escape, we calculated the area under the curve for the estimated kernels excluding the 2 second baseline period using the MATLAB function trapz. We estimated a distribution of AUC from the bootstrapped data and determined that the kernels were significantly different if the confidence interval for the difference in AUC between the events did not contain 0 (alpha = 0.05 with a Bonferonni correction for multiple comparisons).

In a subset of mice, we included the pose estimation data described above in a second model to control for the effects of movement speed on dopamine fluorescence (Figure S6). This model and its quantification are identical to the one described above except that it also included a temporal kernel for crosses occurring during the intertrial interval and a continuous speed regressor.

To quantify changes in event encoding across days (Figure S4), we fit separate models for each mouse and session and calculated the correlation coefficient between the real and estimated ΔF/F for the full model and for reduced models without predictors associated with each event. We then performed a one-way, repeated measures ANOVA on the Fisher z transformation of the correlation coefficients or difference in correlation coefficients.

Deep Learning Classification Decoder

To decode neural correlates associated with behavioral outcomes, we developed a deep learning classifier using an architecture composed of Long Short Term Memory and Fully Convolutional Networks (LSTM-FCN) as previously described.[24] All dopamine recordings for trials occurring on Days 5-7 were used to develop the classifier. Optimal model parameters were determined through a Bayesian hyperparameter optimization.[38] Hyperparameter sweeps were performed using a dataset split ratio of 0.75 and 0.25 for training and testing respectively. Additionally, all models were trained on the same dataset splits for accurate comparisons. Hyperparameter search space was defined as described (Tables S1 and S2) and algorithmically optimized to maximize accuracy on the test dataset. Each model was recorded and analyzed using CometML.[39] The optimal model was then chosen based on test data accuracy.

Please cite this article in press as: Lopez et al., Region-specific nucleus accumbens dopamine signals encode distinct aspects of avoidance learning, Current Biology (2025), https://doi.org/10.1016/j.cub.2025.04.006

Other statistical methods

One-way or two-way ANOVAs or mixed effects analyses comparing NAc region, day, avoid vs escape, or performance level were performed with Tukey's multiple comparisons tests when statistically significant main effects or interactions were found ($p<0.05$) using Prism 10 software ($n = 22$, Figures 1, 2, 3, 4, and S2–S8; GraphPad). Correlations were conducted using simple linear regressions. Statistical information can be found in the main and supplemental figure legends. Standard deviation (SD) values were plotted in all figures except for Figures 4C and 4E *bottom*, as well as Figures S8B and S8D *bottom* which were both plotted with standard error of the mean (SEM).

Current Biology, Volume *35*

Supplemental Information

Region-specific nucleus accumbens dopamine signals encode distinct aspects of avoidance learning

Gabriela C. Lopez, Louis D. Van Camp, Ryan F. Kovaleski, Michael D. Schaid, Venus N. Sherathiya, Julia M. Cox, and Talia N. Lerner

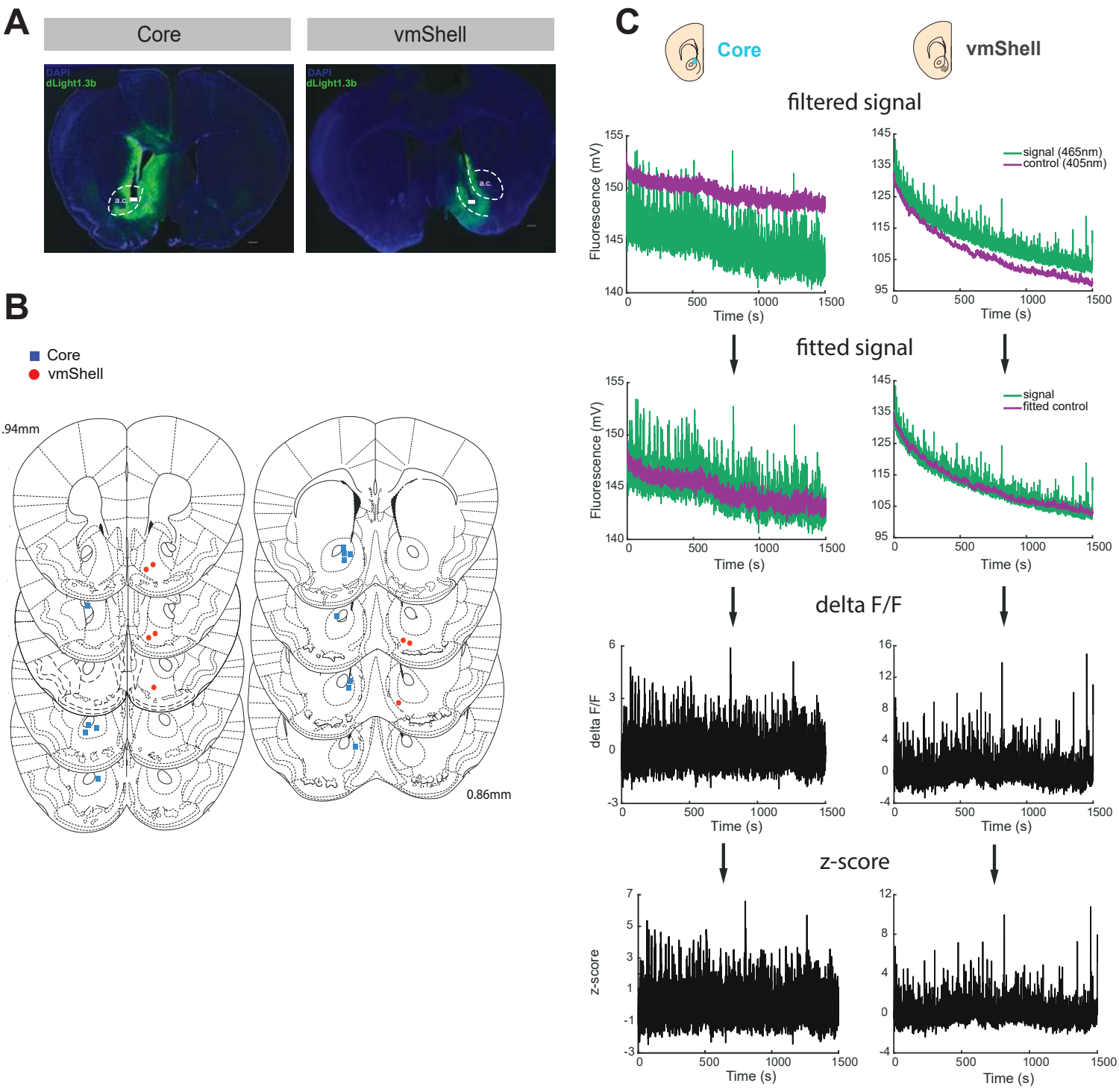
A
Core
vmShell
DAPI
dLight1.3b
a.c.
B
Core
vmShell
1.94mm
0.86mm
C
Core
vmShell
filtered signal
Fluorescence (mV)
Time (s)
signal (465nm)
control (405nm)
fitted signal
signal
fitted control
delta F/F
z-score

Figure S1. Recording sites and processing steps for fiber photometry. Related to Figure 1.

(A) Representative histology images (4x) indicating viral spread of dLight 1.3b (green, all images) and probe placement for Core (left) and vmShell (right). DAPI (blue, all images) was used for nuclear staining. Scale bars are 300 μm; a.c., anterior commissure. Thick white bars indicate probe placement.

(B) Probe placements in Core (blue squares) and vmShell (red circles) for all mice included in Figures 1-4.

(C) Representative signal processing pipeline for Core and vmShell fiber photometry data included in Figures 1-4. Green traces represent dopamine-related fluorescence signals recorded using 465 nm excitation. Purple traces and purple represent control (~isosbestic) signals recorded using 405 nm excitation.

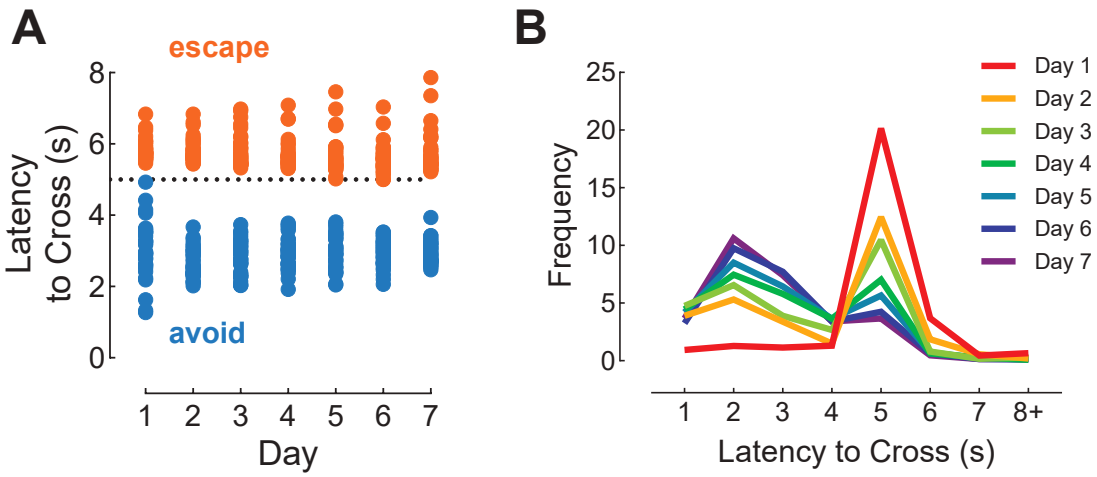
A
escape
avoid
Latency to Cross (s)
0
2
4
6
8
1
2
3
4
5
6
7
Day
B
Frequency
0
5
10
15
20
25
1
2
3
4
5
6
7
8+
Latency to Cross (s)
Day 1
Day 2
Day 3
Day 4
Day 5
Day 6
Day 7

Figure S2. Latency to cross by trial type and frequency. Related to Figure 1.

(A) Latency to cross across days of active avoidance training split by trial type. Orange dots represent average escape trial latencies and blue dots represent average avoid trial latencies for each mouse on each day. After day 1, avoid and escape latencies remained stable, with avoid latencies remaining ~3 s and escape latencies remaining ~< 1s.

(B) Frequency histogram of latency-to-cross times across days of active avoidance training. Mice show a bimodal shift of latencies within 5-6s on early days to latencies within 2-3s on later days of training.

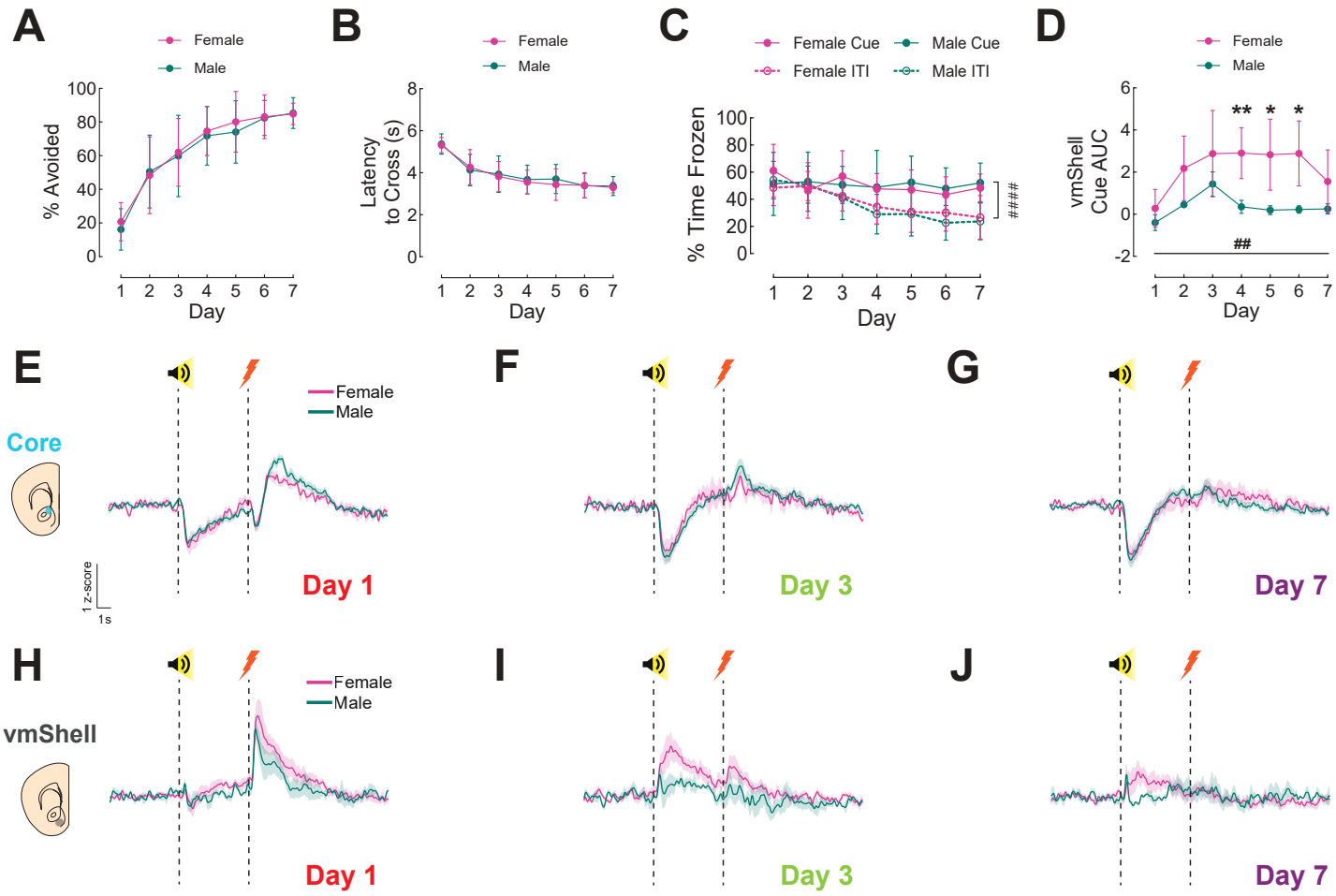
A
Female
Male
% Avoided
Day
B
Female
Male
Latency to Cross (s)
Day
C
Female Cue
Male Cue
Female ITI
Male ITI
% Time Frozen
####
Day
D
Female
Male
vmShell Cue AUC
**
*
*
##
Day
E
Core
Female
Male
1 z-score
1s
Day 1
F
Day 3
G
Day 7
H
vmShell
Female
Male
Day 1
I
Day 3
J
Day 7

Figure S3. Lack of sex differences in NAc Core and vmShell dopamine responses during avoidance learning. Related to Figure 1.

(A) Percentage of shocks avoided over days of active avoidance training split by sex. No significant differences are seen between females (n = 18, pink) and males (n = 18, green) across days of training (mixed effects analysis; $F(1, 34) = 0.2606$, $p = 0.6130$).

(B) Latency to cross over days of active avoidance training split by sex. No significant differences are seen between females (n = 18, pink) and males (n = 18, green) across days of training (two-way ANOVA; $F(1, 34) = 0.1731$, $p = 0.6800$).

(C) Percent time frozen during the cue (solid lines) and ITI (dashed lines) over days of active avoidance split by sex. While there is a significant difference for freezing between cue and ITI (mixed effects analysis; $F(1, 48) = 26.70$, ****$p < 0.0001$), no significant differences are seen between females (n = 12, pink) and males (n = 13, green) across days of training (mixed effects analysis; $F(1, 145) = 0.0007188$, $p = 0.9786$). Hash symbol (#) indicates main effects. Error bars are SD.

(D) Cue AUC for vmShell dLight1.3b signals over days split by sex (females n = 5, males n = 3). While there was a main effect of day, there was no main effect of sex (two-way ANOVA; $F(2.421, 14.53) = 6.469$, $p = 0.0074$ (Day); $F(1, 6) = 5.888$, $p = 0.0514$ (Sex). Days 4, 5, and 6 are significantly different by sex. (Tukey's multiple comparison's test; day 4 male versus female, **$p = 0.0071$, day 5 male versus female, *$p = 0.0240$, day 6 male versus female, *$p = 0.0174$). Hash symbol (#) indicates main effects and asterisk (*) indicate post hoc comparisons. Error bars are SD.

(E-G) Plots showing the dopamine signals collected from Core for females (n = 5, pink) and males (n = 9, green) aligned to the start of the warning cue (first dotted line). Shock occurred 5s after the warning cue start on escape trials (second dotted line). Day 1 (E), Day 3 (F), and Day 7 (G) are shown.

(H-J) Plots showing the dopamine signals collected from vmShell for females (n = 5, pink) and males (n = 3, green) aligned to the start of the warning cue (first dotted line). Shock occurred 5s after the warning cue start on escape trials (second dotted line). Day 1 (H), Day 3 (I), and Day 7 (J) are shown.

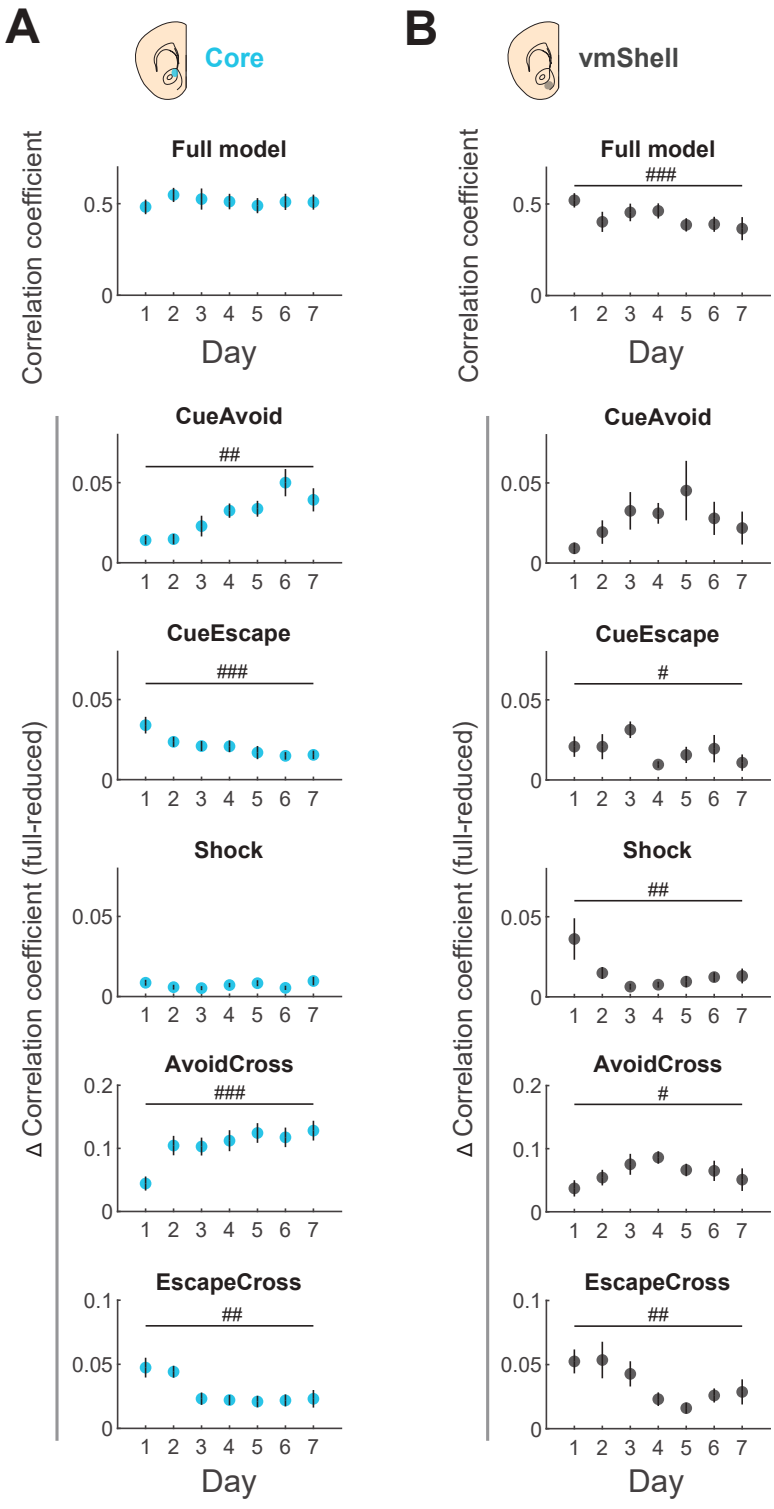
A
Core
B
vmShell
Correlation coefficient
Full model
###
0.5
0
1 2 3 4 5 6 7
Day
Δ Correlation coefficient (full-reduced)
CueAvoid
##
0.05
CueEscape
###
#
Shock
AvoidCross
0.2
0.1
EscapeCross

Figure S4. Analysis of encoding of individual events by modeling dopamine signal in individual mice. Related to Figure 2.

(A,B) Correlation coefficients for the full encoding model (top) of dopamine signal for Core (A) and vmShell (B) show a similar conclusion to Figure 2Q – that Core encoding remains steady over days, while vmShell encoding weakens (one-way, repeated measures ANOVA, $F(6,36) = 4.88$, $p = 9.64 \times 10^{-4}$). The difference in correlation coefficients for the full model compared to a reduced model with each event removed (bottom) show significant changes in representations of various task variables with over days of training.

*p<0.05, **p<0.01, ***p<0.001 for a change over days by one-way, repeated measures ANOVA. Error bars are standard error of the mean.

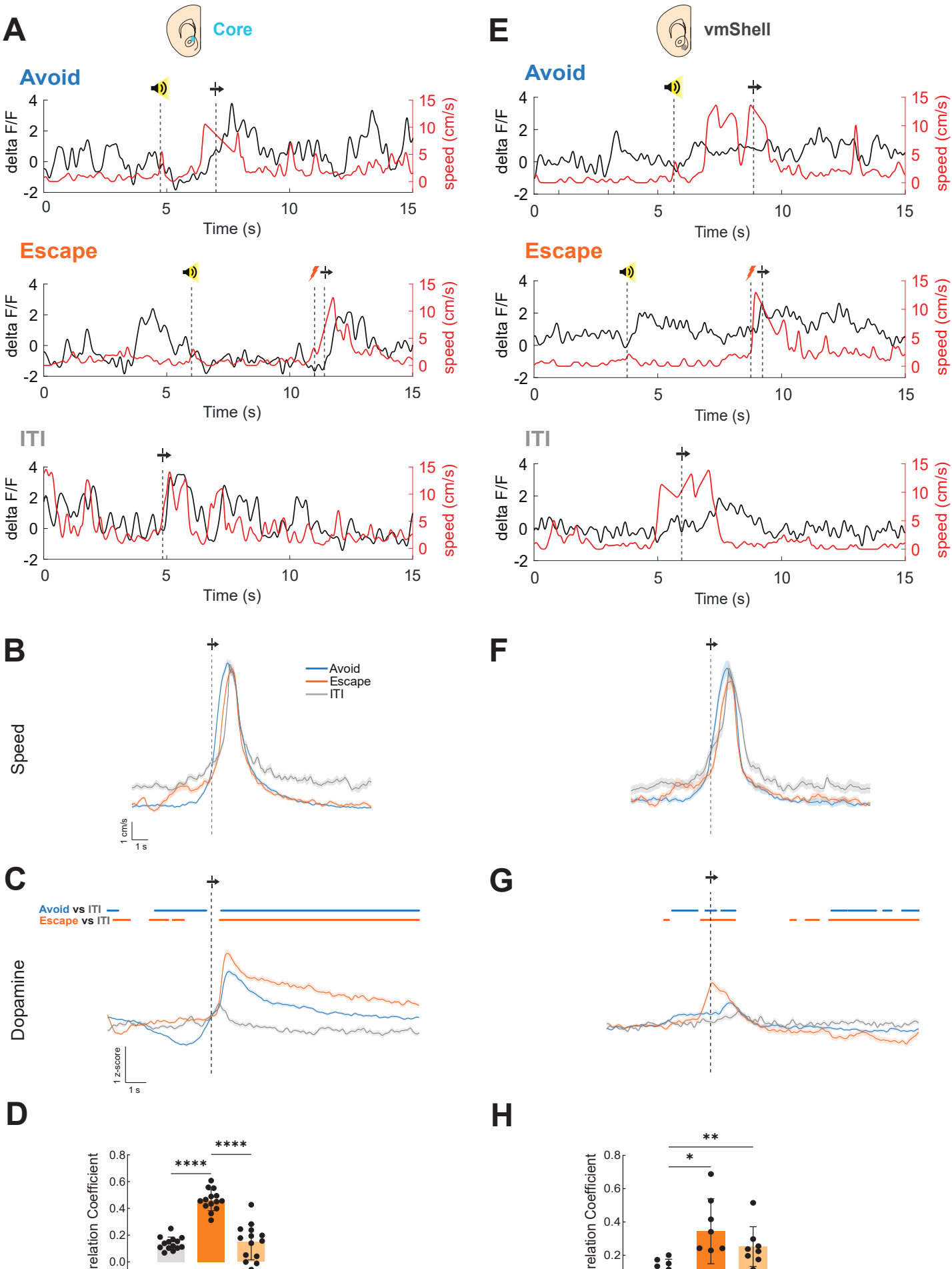
A
Core
Avoid
Escape
ITI
delta F/F
speed (cm/s)
Time (s)
E
vmShell
B
Speed
Avoid
Escape
ITI
1 cm/s
1 s
F
C
Avoid vs ITI
Escape vs ITI
Dopamine
1 z-score
1 s
G
D
Correlation Coefficient
****
****
All
Task
ITI
H
**
*
All
Task
ITI

Figure S5. Correlations of Core and vmShell dopamine signals with speed. Related to Figure 2.

(A,E) Example dopamine signal and speed traces for avoid events (top), escape events (middle), and ITI events (bottom). Black traces represent dopamine signal while red traces represent speed traces. Dashed black lines indicate different time locked events (Cue, Shock, Avoid Cross, Escape Cross, or ITI Cross).

(B,F) Average speed traces for Core mice (B) or vmShell mice (F) aligned to crossing events (avoid, blue; escape, orange; ITI, gray).

(C,G) Average dopamine signal for Core (C) or vmShell (G) aligned to crossing events (avoid, blue; escape, orange; ITI, gray). For C and G, significant deviations from baseline in fiber photometry signals (defined as when the bounds of the 95% CIs did not include 0) are above each plot. Blue lines above traces indicate significant differences between avoid and ITI traces. Orange lines above traces indicate significant differences between escape and ITI traces.

(D,H) Correlations between dopamine signal and speed for Core (D) and vmShell (H) during the entire recording (All) or specific crossing events (avoid or escape crossings = Task; ITI crossings = ITI) or overall movement. Core dopamine signals were significantly more modestly correlated with crossing movements related to the task (avoid or escape crossings) compared to ITI crossings and movement across the entire recording (repeated measures one-way ANOVA; $F (1.368, 17.79) = 64.69$, $p< 0.0001$; Tukey's multiple comparisons, all versus task, ****$p<0.0001$, task versus ITI, ****$p<0.0001$). In the vmShell, dopamine signals were more correlated with speed during both task-specific and ITI crossings than during general overall movement (vmShell; repeated measures one-way ANOVA; $F (1.454, 10.18) = 12.98$, $p = 0.0026$; Tukey's multiple comparisons, all versus task, *$p = 0.0117$, all versus ITI, **$p = 0.0082$). Asterisk (*) indicate post hoc comparisons. Error bars are SD.

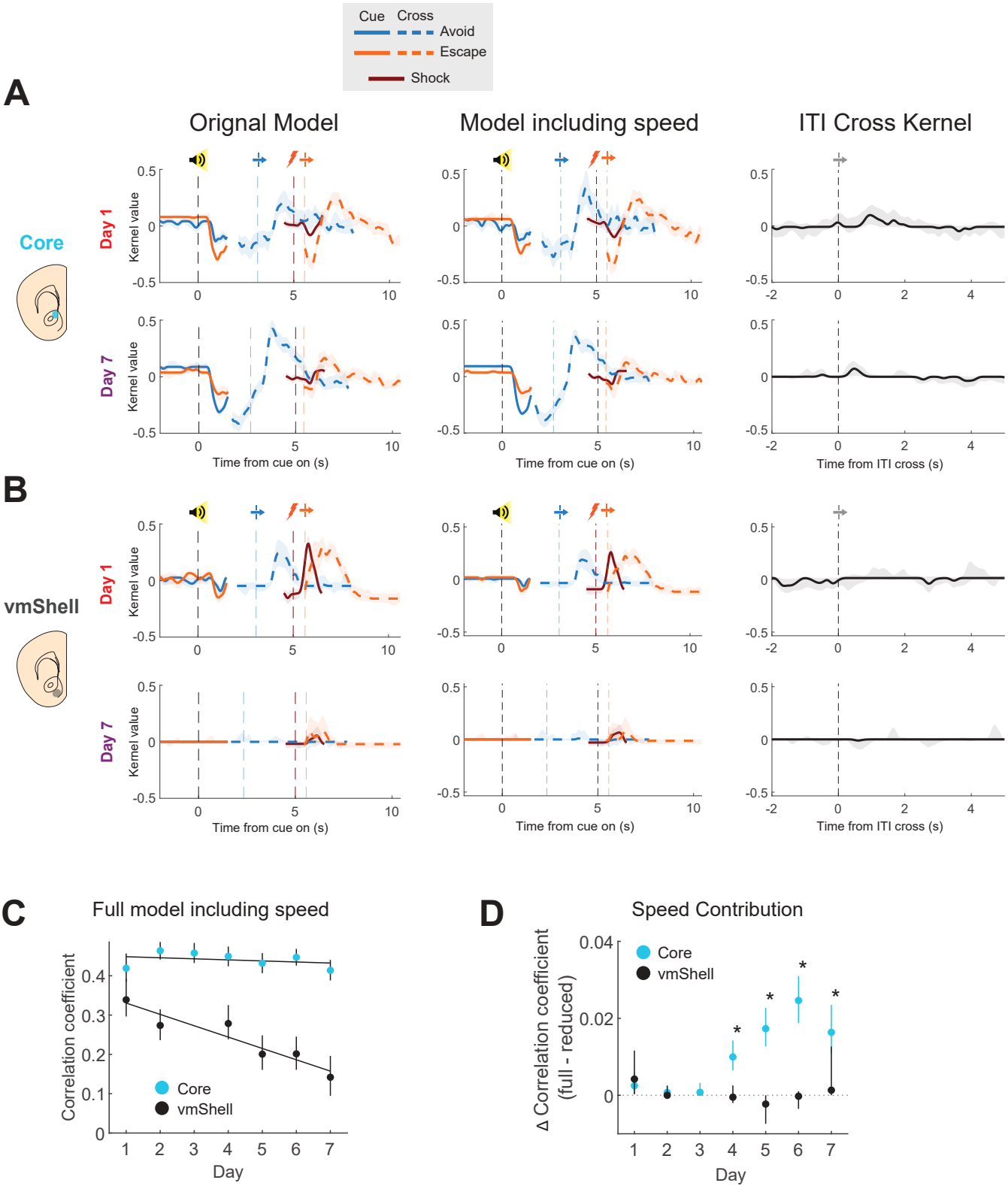
Cue
Cross
Avoid
Escape
Shock
A
Orignal Model
Model including speed
ITI Cross Kernel
Core
Day 1
Day 7
Kernel value
Time from cue on (s)
Time from ITI cross (s)
B
vmShell
C
Full model including speed
Correlation coefficient
Day
Core
vmShell
D
Speed Contribution
Δ Correlation coefficient (full - reduced)

Figure S6. Encoding model including speed as a regressor. Related to Figure 2.

(A,B) Kernel values from the two encoding models of the photometry signals (with and without speed as a regressor) for Core (A) and vmShell (B) are shown for Days 1 and 7 of training. Left, kernel values for the original model (shown in Figure 3). Middle, kernel values including speed as a regressor. Right, kernel values for ITI crossings. For the left and middle plots, behavioral events are marked by vertical dashed lines: cue-on (black), median crossing time for avoid trials (blue), median crossing time for escape trials (orange), shock-on (for escape trials only; dark red). For the plot on the right, the dashed line at 0s indicates ITI cross time.

(C) Correlation coefficients over days for the full encoding models for Core and vmShell dopamine including speed as a regressor. The rate of change is estimated by fitting a line to each set of data points (Core slope = -0.0027, $p = 0.51$; vmShell slope = -0.0299, $p = 0.0046$).

(D) The change in correlation coefficients when speed is removed as a behavioral event (full model – reduced model). Asterisks indicate that the difference in correlation coefficients is significantly different from 0 (dashed line; based on confidence intervals with a Bonferroni correction for multiple comparisons).

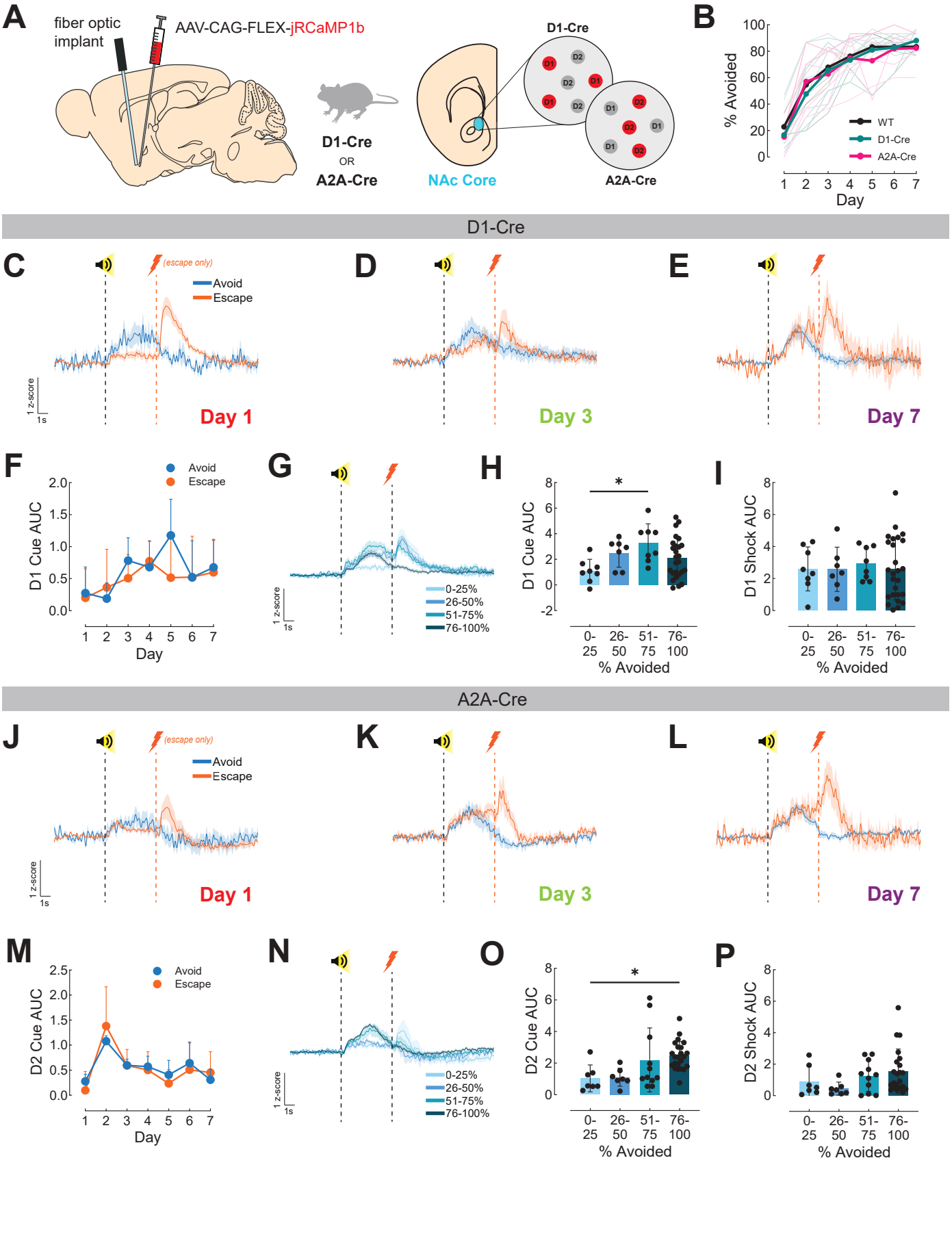
A
fiber optic implant
AAV-CAG-FLEX-jRCaMP1b
D1-Cre
OR
A2A-Cre
NAc Core
D1-Cre
A2A-Cre
B
% Avoided
Day
WT
D1-Cre
A2A-Cre
D1-Cre
C
D
E
(escape only)
Avoid
Escape
1 z-score
1s
Day 1
Day 3
Day 7
F
G
H
I
D1 Cue AUC
D1 Shock AUC
0-25%
26-50%
51-75%
76-100%
% Avoided
A2A-Cre
J
K
L
M
N
O
P
D2 Cue AUC
D2 Shock AUC

Figure S7. Recording from D1- and D2-SPNs in Core during avoidance learning. Related to Figure 3.

(A) Viral strategy for D1- and D2-SPN recordings. An AAV expressing cre-dependent jRCaMP1b was injected into the Core of D1-Cre or A2A-Cre to report calcium activity of D1- or D2-SPNs, respectively. A fiber optic was placed at the same site to allow the collection of fluorescent signals by fiber photometry.

(B) Performance on the active avoidance task split by genotype – Wildtype (WT), D1-Cre, or A2A-Cre. There was no difference in avoidance behavior based on genotype.

(C-E) Plots showing D1-SPN activity (n = 7) collected during avoid trials (blue) and escape trials (orange) from aligned to the start of the warning cue (first dotted line). Shock occurred 5s after the warning cue start on escape trials (second dotted line). Day 1 (B), Day 3 (C), and Day 7 (D) are shown.

(F) The D1-SPN area-under-the-curve (AUC) for the cue period (0-5s) is shown for avoid and escape trials across days. No significant differences are observed between avoid and escape trials (two-way ANOVA; $F(1, 6) = 1.217$, $p = 0.3122$). Error bars are SD.

(G) Cue-aligned D1-SPN signals divided out according to the avoidance performance of the mouse rather than day recorded.

(H) D1-SPN cue AUC by performance level. D1-SPN cue AUC is more significantly different early in training (one-way ANOVA; $F(3, 45) = 3.279$, $p = 0.0294$; Tukey's comparisons; 0-25% versus 51-75% avoidance, $^*p = 0.0187$). Error bars are SD.

(I) D1-SPN shock AUC by performance level. No significant differences are observed between performance levels (one-way ANOVA; $F(3, 45) = 0.09217$, $p = 0.9640$). Error bars are SD.

(J-L) Plots showing D2-SPN activity (n = 7) collected during avoid trials (blue) and escape trials (orange) from aligned to the start of the warning cue (first dotted line). Shock occurred 5s after the warning cue start on escape trials (second dotted line). Day 1 (I), Day 3 (J), and Day 7 (K) are shown.

(M) The D2-SPN area-under-the-curve (AUC) for the cue period (0-5s) is shown for avoid and escape trials across days. No significant differences are observed between avoid and escape trials (mixed effects analysis; $F(1, 6) = 0.03755$, $p = 0.8528$). Error bars are SD.

(N) Cue-aligned D2-SPN signals divided out according to the avoidance performance of the mouse rather than day recorded.

(O) D2-SPN cue AUC by performance level. D2-SPN cue AUC is more significantly different later in training (one-way ANOVA; $F(3, 44) = 3.973$, $p = 0.0137$; Tukey's comparisons; 0-25% versus 76-100% avoidance, $^*p = 0.0432$). Error bars are SD.

(P) D2-SPN shock AUC by performance level. No significant differences are observed between performance levels (one-way ANOVA; $F(3, 43) = 1.877$, $p = 0.1478$). Error bars are SD.

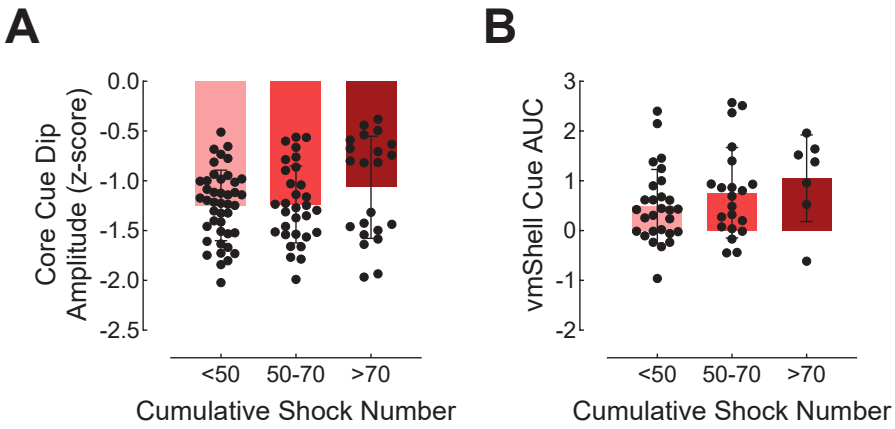
A
Core Cue Dip
Amplitude (z-score)
0.0
-0.5
-1.0
-1.5
-2.0
-2.5
<50
50-70
>70
Cumulative Shock Number
B
vmShell Cue AUC
3
2
1
0
-1
-2
<50
50-70
>70
Cumulative Shock Number

Figure S8. Core and vmShell dopamine cue responses are not altered according to cumulative shock experience. Related to Figure 3.

(A, B) Core cue dip amplitude (A) or vmShell cue AUC (B) based on cumulative shock number across days of training. Each dot represents a session. Multiple sessions from each mouse may be represented in a category. The categories of cumulative shock number (<50, 50-70, >70) on the y-axis were determined by calculating the average number of cumulative shocks experienced by mice across the 7 days of training (~50 shocks) to define the middle and lowest categories and subtracting the average from the max number of experienced shocks (~120 shocks) to define the highest category. For Core, there was no significant difference between shock number and cue dip amplitude (one-way ANOVA; $F(2, 93) = 1.642$, $p = 0.1991$). For vmShell, there was no significant difference between shock number and cue AUC (one-way ANOVA; $F(2, 53) = 1.574$, $p = 0.2168$). Error bars are SD.

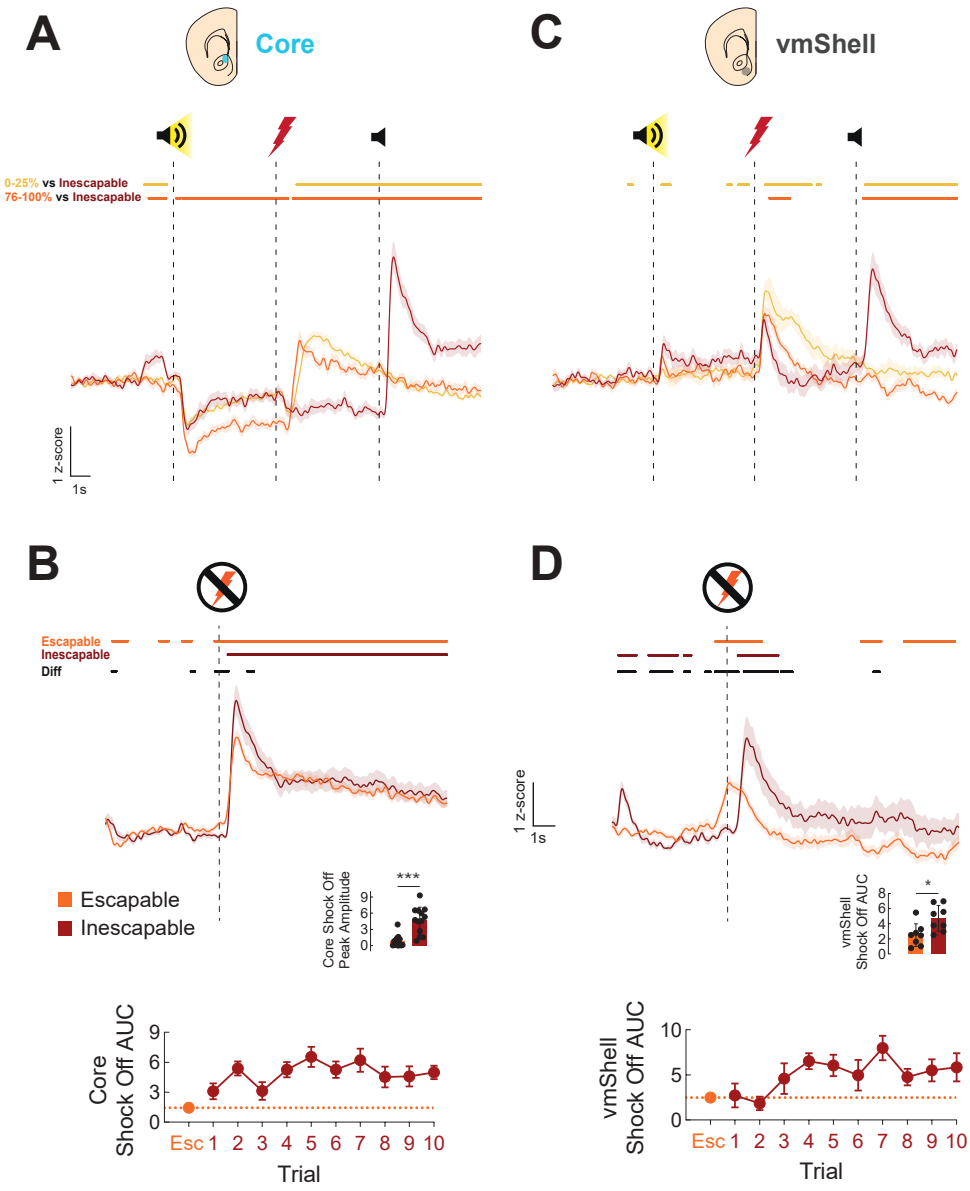
A
Core
0-25% vs Inescapable
76-100% vs Inescapable
1 z-score
1s
C
vmShell
B
Escapable
Inescapable
Diff
Escapable
Inescapable
Core Shock Off Peak Amplitude
***
Core Shock Off AUC
Esc 1 2 3 4 5 6 7 8 9 10
Trial
D
1 z-score
1s
vmShell Shock Off AUC
*
vmShell Shock Off AUC
Esc 1 2 3 4 5 6 7 8 9 10
Trial

Figure S9. Core and vmShell dopamine dynamics differ in response to shock during escapable and inescapable tasks as well as when shock is removed. Related to Figure 4.

(A,C) Comparisons of average dopamine signals aligned to cue for Core (A) and vmShell (C) during escapable and inescapable tasks. Dopamine signals shown from the escapable task are from escape only trials, where animals experienced shock. Dopamine signals during the escapable task are split between low avoidance performance (when animals fail to avoid many shocks, 0-25%) and high or “expert” avoidance performance (when animals successfully avoid most shocks, 76-100%). Dopamine signals for the escapable task during 0-25% performance are shown in mustard yellow and dopamine signals for the escapable task during 76-100% performance are shown in orange. Inescapable task dopamine signals are shown in dark red.

(B,D, *top*) Dopamine signals recorded in Core (B) and vmShell (D) aligned to shock termination for inescapable (orange) or escapable (dark red) shocks.for Core (B) and vmShell (D) in response to controllable or uncontrollable shock termination. The dotted line indicates the time of shock end. The inset shows that shock-off AUC (0-5 s after shock-off) was significantly higher during inescapable shock than escapable shock from high performance days (Core; paired t-test, escapable versus inescapable, $t=4.821$, $df=12$, $p = 0.0004$) (vmShell; paired t-test, escapable versus inescapable, $t=2.490$, $df=7$, $p = 0.0416$).

(B,D *bottom*) Average Core shock off AUC (B) or vmShell shock- off AUC (D) during escapable shock from high performance days (76-100% avoidance days, orange dots) and each of the 10 inescapable shock trials (dark red dots). Orange dotted line indicates shock- off AUC during escapable shock from high performance days for comparison. Shock off AUC was significantly higher during inescapable shock than escapable shock from high performance days (Core; paired t-test, escapable versus inescapable, $t=4.821$, $df=12$, ***$p = 0.0004$) (vmShell; paired t-test, escapable versus inescapable, $t=2.490$, $df=7$, *$p = 0.0416$). Error bars are SD.

Parameter	Value
adam amsgrad	FALSE
adam beta 1	0.9
adam beta 2	0.999
adam clipnorm	null
adam clipvalue	null
adam ema momentum	0.99
adam ema overwrite frequency	null
adam epsilon	1.00E-07
adam global clipnorm	null
adam gradient accumulation steps	null
adam learning rate	0.001
adam loss scale factor	null
adam use ema	FALSE
adam weight decay	null
attention	FALSE
batch size	128
callbacks	null
categories	auto
drop	null
dropout	0.6
dtype	<class 'numpy.float64'>
epochs	1000
feature name combiner	concat
filter sizes	[128,256,128]
handle unknown	error
kernel sizes	[32,15,9]
lstm size	6
max categories	null
min frequency	null
n epochs	2000
Optimizer	adam
random state	42
sparse output	FALSE
verbose	

Table S1. Parameters of optimized Long Short-Term Memory Fully Convolutional Network Model. Related to Figure 2.

algorithm	bayes
maxCombo	30
objective	maximize
metric	test_balanced_accuracy
minSampleSize	700
retryLimit	20
retryAssignLimit	0
epochs	500, 1000, 1500, 2000
dropout	0.2, 0.4, 0.6, 0.8
kernel_sizes	(32, 15, 9) (16, 10, 6), (8, 5, 3)
filter_sizes	(128, 256, 128),(64, 128, 64)
lstm_size	2, 4, 6, 8, 10
random_state	42

Table S2. Hyperparameters Search Space Table for Bayesian optimization of LSTM-FCN. Related to Figure 2.

	Dataset	Value
Accuracy	Test	0.8742
	Train	0.8874
Accuracy (weighted)	Test	0.6774
	Train	0.7403
F1 Score	Test	0.4722
	Train	0.6383
F1 Score (weighted)	Test	0.8651
	Train	0.8741
Precision	Test	0.5667
	Train	0.9
Precision (weighted)	Test	0.8606
	Train	0.8887
ROC-AUC	Test	0.8569
	Train	0.9551
Recall	Test	0.4048
	Train	0.4945
Recall (weighted)	Test	0.8742
	Train	0.88

Table S3. Performance metrics for LSTM-FCN model. Related to Figure 2.